Quaternary Science Reviews 150 (2016) 184–199

Contents lists available at ScienceDirect

Quaternary Science Reviews

journal homepage: www.elsevier.com/locate/quascirev

Evidence for regional cooling, frontal advances, and East Greenland Ice Sheet changes during the demise of the last interglacial

Nil Irvalı [a, b, *], Ulysses S. Ninnemann [a, b], Helga (Kikki) F. Kleiven [a, b], Eirik V. Galaasen [a, b], Audrey Morley [c], Yair Rosenthal [d]

[a] Department of Earth Science, University of Bergen, Allégaten 41, 5007 Bergen, Norway
[b] Bjerknes Centre for Climate Research, Bergen, Norway
[c] Discipline of Geography, National University of Ireland, Galway, University Road, Galway, Ireland
[d] Institute of Marine and Coastal Sciences and Department of Geology, Rutgers, The State University of New Jersey, 71 Dudley Road, New Brunswick, NJ 08901, USA

ARTICLE INFO

Article history:
Received 12 April 2016
Received in revised form
17 August 2016
Accepted 19 August 2016

Keywords:
Eirik drift
Greenland Ice Sheet
North Atlantic
Last interglacial
Glacial inception
Multi-proxy

ABSTRACT

High-resolution lithic and sea surface climate records are used to portray the progression of North Atlantic climate, hydrography, and Greenland Ice Sheet (GIS) activity through the peak of Marine Isotope Stage (MIS) 5e into the last glacial inception. We use Eirik Drift sediment core MD03-2664 (57°26.34′N, 48°36.35′W), recovered south of Greenland, strategically located to monitor fluctuations in GIS extent and iceberg calving events. Our results show that a significant amount of ice-rafted debris (IRD) was present during the early MIS 5e, until gradually tapering off by 122 kyr BP due to a diminishing GIS. Sea surface temperatures (SSTs) in the northern subpolar gyre reached peak values early in MIS 5e coinciding with peak insolation. Regional cooling leading to the demise of the last interglacial started prior to the end of the MIS 5e benthic $\delta^{18}O$ plateau, at approximately 119 kyr BP, as summer insolation waned. This gradual cooling trend is interrupted by an abrupt and brief cooling episode at ~117 kyr BP. Increased IRD abundance during the 117 kyr BP cooling event suggests that regional ice sheet growth occurred prior to the end of the MIS 5e benthic $\delta^{18}O$ plateau, and the major glacial inception. SSTs south of Greenland followed a two-step cooling during the glacial inception similar to the pattern observed across much of the North Atlantic and Europe. Benthic $\delta^{18}O$ increases in parallel, suggesting that this two-step cooling is linked to a two-phased intensification of Northern Hemisphere glaciation.

1. Introduction

The last glacial inception is characterized by significant cooling of the high latitudes, and the advance of Northern Hemisphere ice sheets amplified by the declining Northern Hemisphere summer insolation. The evolution of climate and ice sheets through this important transition provides insight into climate and ice sheet sensitivity. Under what forcing conditions do ice sheets nucleate and which areas are most sensitive? There is indirect evidence from sea level records (e.g., Thompson et al., 2011) that ice sheets do vary during interglacials, and that these variations may become more significant/larger in amplitude as Northern Hemisphere summer insolation wanes. Yet the loci of ice sheet growth/variability remains poorly constrained due to the limited number and distribution of records constraining past ice sheet changes.

A frequently used proxy for ice sheet variability is ice-rafted debris (IRD), which comprises lithic grains transported by calving glaciers that drift and melt with prevailing ocean currents. Therefore, the presence of icebergs is the determining factor for IRD deposition at any given location, and the amount of IRD is attributed to the supply rate of calving glaciers (Jansen et al., 2000). Indirectly, the presence of IRD in pelagic sediments thus provides evidence for marine terminating glaciers at the time of deposition. Detailed studies of sediment cores from the Nordic Seas and subpolar North Atlantic, that span the last glacial cycle have documented that there is a high degree of correlation between the advance of ice sheets and the magnitude of IRD peaks in open ocean sediments (Baumann et al., 1995; Dokken and Jansen, 1999; Fronval et al., 1995; King et al., 1996; Mangerud et al., 1996; Sejrup et al.,

* Corresponding author. Department of Earth Science, University of Bergen, Allégaten 41, 5007 Bergen, Norway.
E-mail address: nil.irvali@uib.no (N. Irvalı).

http://dx.doi.org/10.1016/j.quascirev.2016.08.029

2000). IRD records therefore provide a means to reconstruct ice sheet dynamics and their interaction with the climate system, providing evidence of both source and location of ice sheet melting (Bond and Lotti, 1995; Ruddiman, 1977).

North Atlantic IRD records spanning the last interglacial suggest the following sequence of events: a high and variable IRD deposition characterizing late Marine Isotope Stage (MIS) 6; a significant increase in IRD marking a massive iceberg discharge associated with Heinrich Event 11 (H11) at the end of MIS 6; a reduction to near-zero IRD abundance through MIS 5e; and generally low abundances until late MIS 5d, followed by a well-known sequence of IRD events through the rest of MIS 5 (i.e., cold episodes C24-19) (Bauch and Kandiano, 2007; Chapman and Shackleton, 1999; Hibbert et al., 2010; McManus et al., 1994; Oppo et al., 2001, 2006). Climatic instability in the North Atlantic during the youngest substages of MIS 5 (5a-5d) was documented by McManus et al. (1994), based on increases in both the IRD content and the abundance of the polar planktonic foraminifera *Neogloboquadrina pachyderma* (sinistral), which suggested advance of polar waters and rapid growth of Northern Hemisphere glaciers (e.g., McManus et al., 1994). Related abrupt cooling and IRD events were later documented for the MIS 5e/5d transition and also within MIS 5e (Chapman and Shackleton, 1999; Mokeddem et al., 2014; Oppo et al., 2001, 2006). However, variations in the spatial distribution and magnitude of these cooling and IRD episodes exist within the North Atlantic.

Evidence from the Nordic Seas and subpolar North Atlantic IRD records indicate that tidewater glaciers reached the margins of the Nordic Seas within MIS 5e, suggesting a relatively early initial growth of regional ice sheets (e.g., Fronval and Jansen, 1997; Oppo et al., 2006). These early increases in IRD during MIS 5e were interpreted as increased influence of polar waters, possibly influenced by solar forcing (Bond et al., 2001), whereas larger events following the glacial inception involved ice sheet instability (Chapman and Shackleton, 1999).

Here, we present new high-resolution multi-proxy records from the Eirik Drift—a high accumulation rate site off southern Greenland, which lies in an important and under-constrained region within the northern Subpolar Gyre (SPG). In particular, the location is ideal for identifying the initial southward incursions of polar water and ice rafted material due to its proximity to the modern polar and arctic fronts and to the southward transport trajectory of icebergs calved from Eastern Greenland's tidewater glaciers. Here we adopt the definition of Polar Front as the boundary between Polar and Arctic waters, and Arctic Front as the boundary between Arctic and Atlantic waters (Swift and Aagaard, 1981). High-resolution lithic and surface climate records from Eirik Drift, together with previously documented records from the Nordic Seas and subpolar North Atlantic, provide new constraints on the co-evolution of North Atlantic climate, hydrography and ice sheet changes in unprecedented detail during the demise of the last interglacial.

2. Core location and oceanographic setting

New high-resolution lithic and sea surface climate records are obtained from the Eirik sediment drift core MD03-2664 (57°26.34′N, 48°36.35′W, 3442 m water depth), which is situated 370 km southwest of Cape Farewell in the Labrador Basin (Fig. 1). This site is sensitively situated with respect to the Greenland Ice Sheet (GIS) and provides the temporal fidelity necessary to detect abrupt perturbations to regional hydrography and climate during the evolution and demise of the last interglacial period. In order to place these changes into a regional context, differentiate between local and regional influences, and map the spatial progression of frontal systems and SPG geometry, the new records are compared with published records from Ocean Drilling Program (ODP) Site 980 and core NEAP-18K from the northern North Atlantic Ocean and core HM57-7 from the Iceland Sea (Chapman and Shackleton, 1999; Fronval and Jansen, 1997; Oppo et al., 2006) (Fig. 1; Table 1).

The Eirik sediment drift accumulates rapidly as a result of the influx of sediments eroded from the Denmark Strait and eastern Greenland margin suspended in Denmark Strait Overflow Water (DSOW) (Wold, 1994). DSOW combines with North West Atlantic Deep Water (NWADW) to form the Western Boundary Undercurrent (WBUC) (McCartney, 1992). Core site MD03-2664 lies just below the main axis of the sediment-laden WBUC and hence preserves expanded interglacial sediment sequences (Hillaire-Marcel et al., 1994).

MD03-2664 is located at the northern edge of the SPG which dominates the surface water hydrography of the northern North Atlantic (Hátún et al., 2005) (Fig. 1). The North Atlantic Current (NAC) forms the eastern segment of the gyre, carrying warm and saline waters northward, while the southward flowing, cold and fresh East Greenland Current (EGC) dominates the western boundary. The EGC, together with the smaller East Greenland Coastal Current (EGCC), are the major contributors of cold and fresh water masses to the vicinity of the study area (Bacon et al., 2002). However, the main component of these currents is deflected and turns northwards around the slope region near Cape Farewell and does not currently extend as far south as the core location (Cuny et al., 2002). Thus, modern surface water properties at the core site primarily reflect the water masses that occupy the interior of the Labrador Basin, which are more stable and less directly influenced by freshwater anomalies in the slope areas (Houghton and Visbeck, 2002).

3. Material and methods

3.1. Sample preparation

The giant piston core (Calypso) MD03-2664 was recovered during the P.I.C.A.S.S.O cruise of the R/V *Marion Dufresne* of the French Institut Polaire Paul Emile Victor (IPEV) within the framework of the International Marine Global Changes (IMAGES) program. MD03-2664 was continuously subsampled at 1-cm spacing over the 5-m long core interval (from 23.5 to 28.5 m) spanning late Marine Isotope Stage (MIS) 6 to early MIS 5d. Each sample was soaked in distilled water and shaken for 12 h in order to disperse the sediment, before they were wet sieved and separated into size fractions of >63 μm and <63 μm. The >63 μm fraction was used for selection of foraminiferal specimens for stable isotope analysis, Mg/Ca analysis, foraminiferal census counts and ice rafted debris (IRD) counts after additional dry sieving. In Figs. 2 and 6 we mark the new MD03-2664 data (this study) with filled circles, whereas previously published data from this core (Galaasen et al., 2014; Irvalı et al., 2012) are marked with open circles.

3.2. Stable isotopes

The planktonic foraminifer species *Neogloboquadrina pachyderma* (sinistral) and benthic foraminifer *Cibicidoides wuellerstorfi* were selected for stable isotope analyses ($\delta^{18}O$ and $\delta^{13}C$) to reconstruct surface and deep ocean physical and chemical properties (Fig. 2a) (Galaasen et al., 2014; Irvalı et al., 2012). *N. pachyderma* (s) was picked every 1 cm (2350–2850 cm) from the 150–250 μm size fraction (7–9 specimens per analysis), while *C. wuellerstorfi* was picked from all size fractions >150 μm (1–2 specimens per analysis). Before analyses, the foraminiferal shells were ultrasonically rinsed for 20 s in methanol to remove fine-

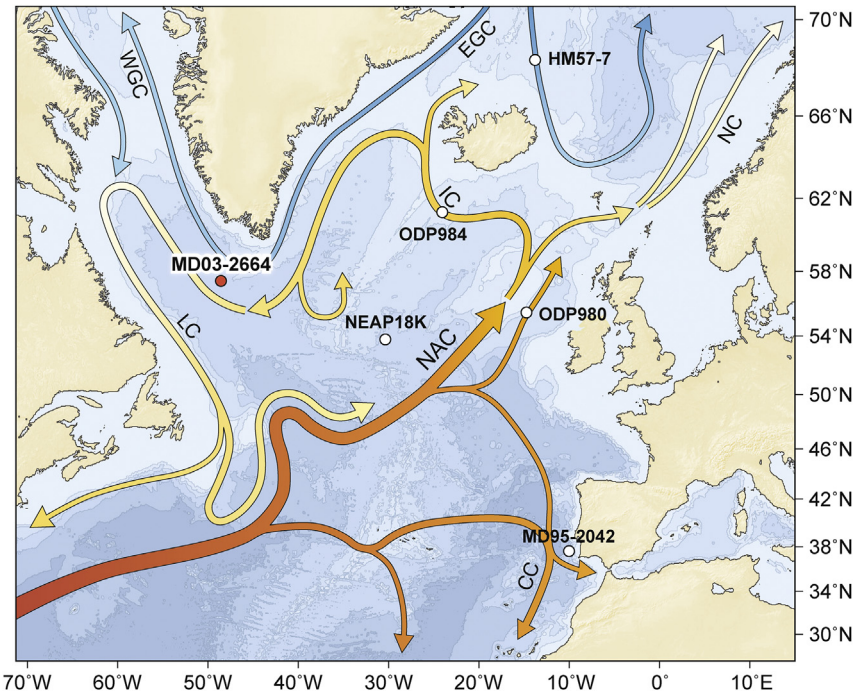

Fig. 1. Map of the North Atlantic Ocean and Nordic Seas with arrows indicating the schematic circulation and spreading pathways of the surface currents in the region that form a portion of the Atlantic Meridional Overturning Circulation. The location of core MD03-2664 is marked with a red circle, and the other cores discussed in the text (ODP Site 980 (Oppo et al., 2006), ODP Site 984 (Mokeddem et al., 2014), NEAP-18K (Chapman and Shackleton, 1999), HM57-7 (Fronval and Jansen, 1997) and MD95-2042 (Shackleton et al., 2000)) are all marked with white circles. (NAC: North Atlantic Current; CC: Canary Current; NC: Norwegian Current; IC: Irminger Current; EGC: East Greenland Current; WGC: West Greenland Current; LC: Labrador Current).

Table 1
Core locations.

Core name	Latitude	Longitude	Water depth	Reference
HM57-7	68°26′N	04°34′E	1620 m	Fronval and Jansen (1997)
ODP984	61°15′N	24°02′W	1648 m	Mokeddem et al. (2014)
MD03-2664	57°26′N	48°36′W	3440 m	This study
ODP980	55°29′N	14°42′W	2179 m	Oppo et al. (2006)
NEAP18K	53°46′N	30°21′W	3175 m	Chapman and Shackleton (1999)
MD95-2042	37°48′N	10°10′W	3146 m	Shackleton et al. (2000)

grained particles. Stable isotope analyses were measured using a Finnigan MAT253 mass spectrometer in the GMS-laboratory at the Department of Earth Science and the Bjerknes Centre for Climate Research, University of Bergen. All samples were run in two replicates whenever foraminifera were sufficiently abundant. Results are expressed as the average of the replicates and reported relative to Vienna Pee Dee Belemnite (VPDB), calibrated using NBS-19 and crosschecked with NBS-18. Long-term reproducibility (1σ) of in-house standards for samples between 10 and 100 μg is better than 0.08‰ and 0.03‰ for $\delta^{18}O$ and $\delta^{13}C$ respectively.

3.3. Lithic counts

Relative abundance of IRD in the >150 μm fraction was counted every 4 cm through the core, as an index for the presence of icebergs. The results are expressed as the percentages of IRD grains relative to total entities (i.e., foraminifera) in each sample (IRD%) (Fig. 2b). The 2400–2850 cm interval of the record has been published previously (Galaasen et al., 2014; Irvalı et al., 2012), here we extend the records further back into MIS 5d, adding the 2350–2400 cm interval, and increase the resolution to every 2 cm for the 2410–2442 cm interval to provide detailed perspectives during the end of the last interglacial period and the glacial inception.

3.4. Foraminiferal counts

Planktonic foraminiferal assemblages were counted every 4 cm throughout the core. The 2410–2442 cm interval was analyzed with a higher resolution (every 2 cm), similar to the IRD counts. Early MIS 5e and MIS 6 intervals (2570–2850 cm) of foraminiferal assemblage data have been shown in Irvalı et al. (2012), here we extend the records further by adding the 2350–2570 cm interval of the core MD03-2664. Each sample was dry-sieved at >150 μm and then split to give at least 300 planktonic foraminifera for census counts. The absolute number of planktonic foraminifera counted ranged from 247 to 936. The most abundant species were *N. pachyderma* (s), *Neogloboquadrina incompta*, *Turborotalia quinqueloba*, *Globigerina bulloides* and *Globigerinita glutinata*. Here we adopt the name *N. incompta* for the dextral coiling *N. pachyderma* variety as suggested by Darling et al. (2006). We use both the relative abundance (%) and coiling ratio of *N. pachyderma* (s). The coiling ratio of *N. pachyderma* (i.e., the percentage of the sinistral coiling variety in total *N. pachyderma* (sinistral + dextral coiling))

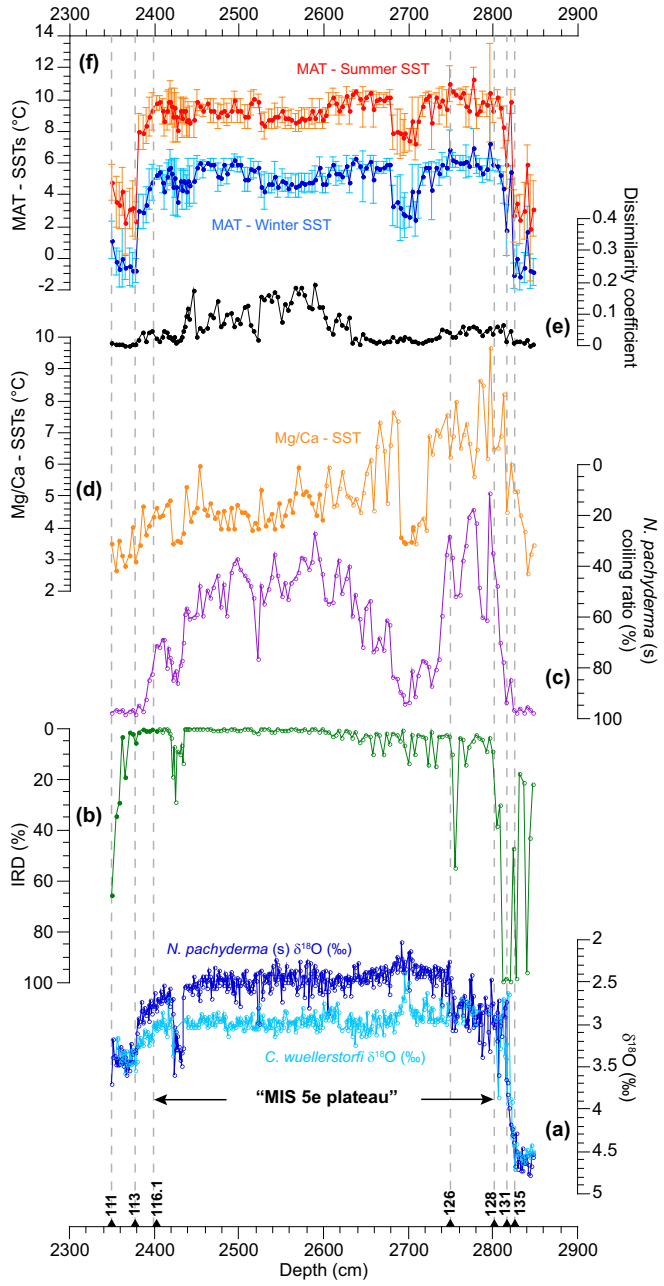

Fig. 2. Proxy records along the MIS 5e section of core MD03-2664 plotted versus depth. **(a)** Benthic (light blue) and planktonic (dark blue) $\delta^{18}O$ records; **(b)** IRD% (green); **(c)** *N. pachyderma* (s) coiling ratio (%) (purple); **(d)** Mg/Ca SSTs (orange); **(e)** Dissimilarity coefficients of SST estimates (black); and **(f)** Summer (red) and Winter (blue) SST estimates from MAT; all plotted versus depth (cm) scale. Error bars on the MAT SST estimates are the standard deviation of the estimates from top five analogs. Dashed vertical lines and triangles denote the calibration points used to construct the age model. Open circles mark the previously published MD03-2664 data (Galaasen et al., 2014; Irvali et al., 2012), whereas filled circles mark new data (this paper). (For interpretation of the references to colour in this figure legend, the reader is referred to the web version of this article.)

(Fig. 2c), is commonly used to infer changes in sea surface temperatures (SST) at high latitudes as the sinistral coiling *N. pachyderma* is dominant in cold/polar regions, whereas the dextral coiled form is found in more temperate/subpolar regions. The abundance records (e.g., of *N. pachyderma* (s), *T. quinqueloba* and *N. incompta*) provide information about the position of frontal systems (Alonso-Garcia et al., 2011; Fronval et al., 1998; Mokeddem et al., 2014; Wright and Flower, 2002). *N. pachyderma* (s) is the most dominant species in Polar and Arctic waters, whereas *T. quinqueloba* is associated with the Arctic Front, as the maximum abundance of this species is observed on the warm side (east) of the Arctic Front (Johannessen et al., 1994). Here we use planktonic foraminiferal assemblages to reconstruct advances and retreats of the Arctic and Polar fronts over the last interglacial. Finally, the abundance of species associated with high productivity, such as *G. bulloides* and *G. glutinata* (e.g., Kucera et al., 2005) are used to monitor associated changes in subpolar productivity.

3.5. Sea surface temperature reconstructions

SSTs were reconstructed using both Mg/Ca paleothermometry and the Modern Analog Technique (MAT) (Fig. 2d, e and 2f). Here we extend the previously published Mg/Ca record of MD03-2664 (2600–2850 cm, Irvali et al., 2012) into the late MIS 5e and MIS 5d by analyzing the 2350–2600 cm interval of the core. Mg/Ca measurements were performed every 4 cm throughout the core, on the planktonic foraminifera *N. pachyderma* (s), picked from the same samples used for stable isotopic and faunal analyses. *N. pachyderma* (s) is a polar species, abundantly found in the upper 50–100 m, although it can also calcify at depths between 100 and 200 m (Bauch et al., 1997; Jonkers et al., 2010; Simstich et al., 2003). *N. pachyderma* (s) blooms during the spring and in late summer (e.g., Jonkers et al., 2010), and therefore the Mg/Ca analyses from *N. pachyderma* (s) would reflect spring or late summer SSTs. However, at ~100–200 m there is little change in seasonal temperatures as these depths lie below the summer/seasonal thermocline. Therefore *N. pachyderma* (s) based SST records (e.g. Mg/Ca) may also reflect annual or winter changes depending on depth habitat, consistent with our Mg/Ca based SSTs giving similar values to MAT reconstructed winter SSTs (Fig. 5). Samples consisting of ~40 individuals selected from the 150–250 μm fraction were gently crushed between two clean glass slides under a microscope to open the individual chambers, and transferred into acid-leached vials. The crushed foraminiferal tests were cleaned to remove various contaminating phases. The cleaning protocol used involved clay removal, followed by reductive and oxidative steps to remove metal oxides and organic matter respectively, weak acid leach and final dissolution in dilute HNO_3. Measurements were carried out on a Finnigan MAT Element XR Sector Field Inductively Coupled Plasma Mass Spectrometer (ICP-MS), following the method outlined by Rosenthal et al. (1999), at the ICP-MS laboratory at the Institute of Marine and Coastal Sciences, Rutgers, The State University of New Jersey, USA. Foraminiferal Fe/Ca and Al/Ca ratios were low throughout the core (typically <100 μmol/mol for both ratios) suggesting negligible contamination from adhered sediment; only one out of 126 samples was rejected because of possible contamination. Six previously analyzed samples (2690, 2694, 2696, 2703, 2704 and 2705 cm) suspected of possible contamination discussed in Irvali et al. (2012) were also reanalyzed and contamination was removed during enhanced cleaning procedures that included repeated hot water baths and sonication during clay removal. We converted our Mg/Ca data to temperature estimates using the linear core-top calibration equation developed by Kozdon et al. (2009) (Fig. 2d), which is based on the correlation with calcification temperatures inferred from Ca isotopes between 3 °C and 6 °C. To account for the difference in the cleaning protocol (reductive step), we corrected the intercept in the original calibration of Kozdon et al. (2009) by −10% (Meland et al., 2006; Rosenthal et al., 2004) and use the following equation: $Mg/Ca = 0.13T + 0.32$. The choice of this equation and the limitation of the calibration is discussed in detail in Irvali et al. (2012). Considering all the

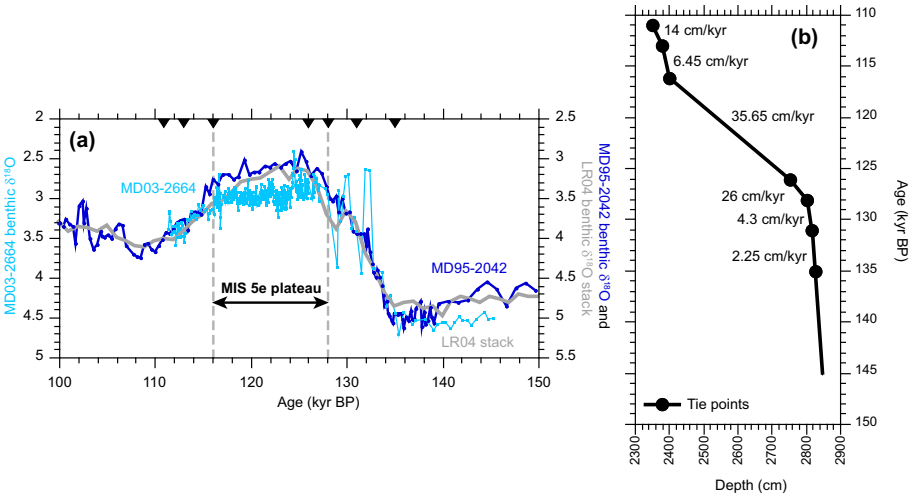

Fig. 3. **(a)** MD03-2664 benthic $\delta^{18}O$ (light blue) record plotted together with MD95-2042 benthic $\delta^{18}O$ (dark blue) record (Shackleton et al., 2000) and the LR04 benthic $\delta^{18}O$ stack (light gray) (Lisiecki and Raymo, 2005) versus age (kyr BP). MD03-2664 and MD95-2042 are plotted versus age model after (Shackleton et al., 2002; Shackleton et al., 2003). Triangles mark the age control points used for MD03-2664. Dashed lines mark the MIS 5e benthic $\delta^{18}O$ plateau. **(b)** Age (kyr BP) – Depth (cm) plot for MD03-2664, showing tie points and sedimentation rates. (For interpretation of the references to colour in this figure legend, the reader is referred to the web version of this article.)

uncertainties in the calibration, the error on the combined calibration is about ±0.4 °C (1 SEE) for temperatures >3 °C.

SST estimates were also calculated from the planktonic foraminiferal census counts, using the MAT (Hutson, 1980; Prell, 1985) (Fig. 2f). In Irvalı et al. (2012) we used the modern core top faunal and SST data from the 527 Atlantic cores in the Brown University core top database (Prell, 1985) to reconstruct the SSTs during the early MIS 5e through the MIS 6 (2600–2850 cm) interval of Core MD03-2664. Here we use the MARGO Project database for the North Atlantic, which consists of 862 samples (Kucera et al., 2005). Although the resulting trends of MAT SST reconstructions based on both databases are similar, the higher number of core-tops located in the North Atlantic in the MARGO database increases the quality of the available analogs. Thus, the current reconstruction supersedes and may be an improvement on the subsets previously presented in Irvalı et al. (2012) or Galaasen et al. (2014) since the MAT is strongly dependent on the size and coverage of the modern database (Kucera et al., 2005). We reconstruct SSTs through the core at 4 cm resolution for 2350–2850 cm, and at 2 cm resolution for the 2410–2442 cm glacial inception interval. Modern SST values at sample locations were computed following Kucera et al. (2005) using the WOA 98 Sample software (http://www.palmod.uni-bremen.de/~csn/woasample.html), which gives the area-weighted average of the four WOA temperature points surrounding the sample locations at 10 m water depth. The program Analog (Prell et al., 1999) was used to match the foraminiferal assemblage at MD03-2664 with the assemblages found in the modern core top database, using the squared chord distance (SCD) as the dissimilarity measure (Prell, 1985). Core tops with dissimilarity greater than 0.4 were not considered. A high dissimilarity coefficient indicates poor modern analogs, with no similar analog existing in the core-top database. At site MD03-2664, the average dissimilarity coefficient through the 2350–2850 cm interval is 0.055 with a standard deviation of 0.01. The averages of summer and winter SST standard deviations are 0.8 °C and 0.89 °C respectively. Low dissimilarity coefficients (≤0.1) derived from the five best analogs suggest reliable SST estimates through the core. Higher dissimilarity coefficients (0.1–0.2) for a few samples in the 2440–2600 cm interval (Fig. 2e) suggest lower confidence in the estimates for these samples.

4. Stratigraphy

Shackleton et al. (2002, 2003) used the marine sediment core MD95-2042 from the Iberian Margin to develop a radiometrically constrained time scale for MIS 5 that is independent of astronomical calibration. Based on Stirling et al's. (1998) age estimates for the MIS 5e sea level high stand, Shackleton and co-workers set the beginning of the MIS 5e "plateau" (defined as the period of low and relatively constant benthic $\delta^{18}O$) at 128.0 ± 1 kyr BP, and the termination of the plateau at 116.1 ± 1 kyr BP. Here we use Shackleton et al's. (2003) benthic $\delta^{18}O$ plateau as an important relative reference point to constrain the period prior to the initiation of significant continental ice sheet growth and/or deep ocean cooling responsible for the benthic $\delta^{18}O$ increase marking the MIS 5e/5d transition. We therefore tuned the benthic $\delta^{18}O$ records of core MD03-2664 (Galaasen et al., 2014) to core MD95-2042 and assigned calibration points at 135.0 kyr BP, 128.0 kyr BP, 116.1 kyr BP, and 113.0 kyr BP based on the benthic $\delta^{18}O$ signal (Figs. 2a and 3). We refined this tuning further, by also comparing the planktonic $\delta^{18}O$ records of MD95-2042 and MD03-2664, and assigning an additional calibration point at 126.0 kyr BP, based on an abrupt planktonic $\delta^{18}O$ shift described by Shackleton et al. (2003) that is also evident in MD03-2664 (Irvalı et al., 2012). We note that the addition of 126 kyr BP tie point changes the age model by less than 500 years and thus the shift in planktonic records are coeval within the uncertainty of the age model even if this age control point is not adopted. This abrupt shift in the MD95-2042 planktonic $\delta^{18}O$ record at ~126 kyr BP is coeval with the beginning of the Eemian Interglacial on land, which occurs ~2 kyr after the beginning of the MIS 5e benthic $\delta^{18}O$ plateau (Shackleton et al., 2003). Finally, based on the revised radiometric ages from precisely dated speleothem records (Cheng et al., 2009; Drysdale et al., 2007), we assign 131 kyr BP to the Heinrich Event 11 (H11), and 111 kyr BP to the large IRD peak (at 2350 cm) corresponding to the C24 event (Hodell et al., 2009; McManus et al., 1994; Rousseau et al., 2006)), following the assumption that these events should be synchronous throughout the North Atlantic (Capron et al., 2014; Mokeddem et al., 2014; Tzedakis et al., 2012). As a result we have updated the age model for MD03-2664 used by Galaasen et al. (2014) by assigning a revised age for the C24 event and adding a new tie point for the H11 event.

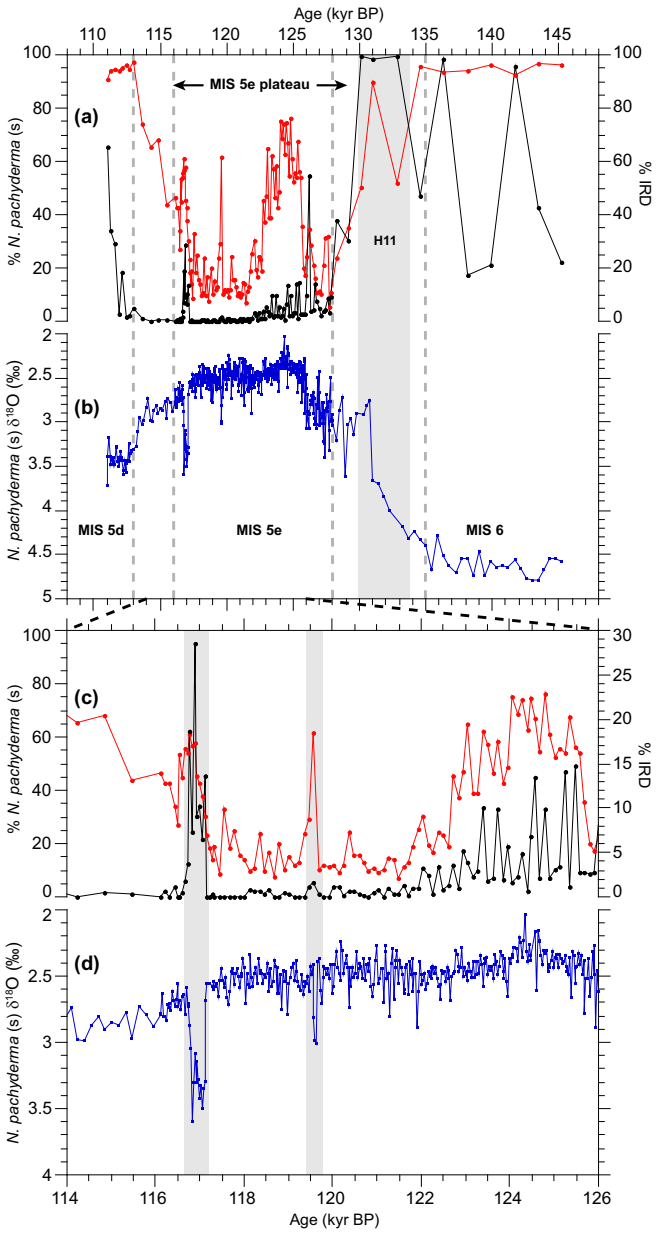

Fig. 4. Surface water proxy records along core MD03-2665 plotted versus age (kyr BP). The two top panels (a and b) span the full study interval from 108 to 148 kyr BP, whereas the two bottom panels (c and d) are focused over the 114–126 kyr BP interval. **(a)** IRD% (black) and relative abundance of *N. pachyderma* (s) % (red) plotted together; **(b)** *N. pachyderma* (s) $\delta^{18}O$ record (dark blue); **(c)** IRD% (black) and relative abundance of *N. pachyderma* (s) % (red) plotted together, **(d)** *N. pachyderma* (s) $\delta^{18}O$ record (dark blue). The gray dashed vertical lines in the upper panels (a and b) denote the calibration points used to construct the age model, and the MIS 5d/5e substage and MIS 5e/6 boundaries. Gray shadings in the bottom panels (c and d) indicate the brief cooling events respectively at 117 and 119.5 kyr BP. (For interpretation of the references to colour in this figure legend, the reader is referred to the web version of this article.)

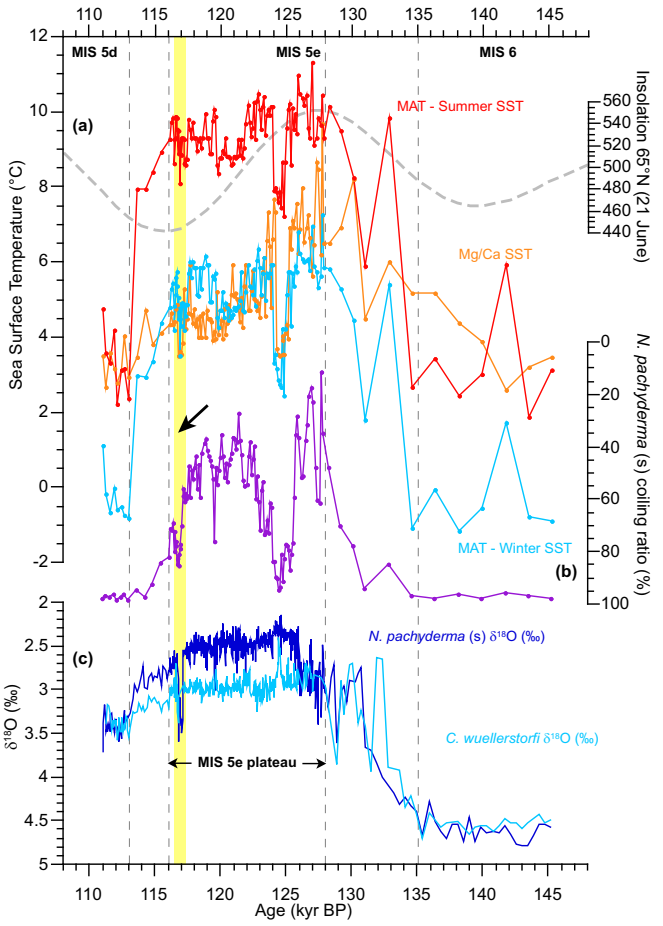

Fig. 5. Proxy records along core MD03-2664 plotted versus age (kyr BP), plotted together with the summer (21 June) insolation at 65°N (Laskar et al., 2004). The dashed vertical lines denote the calibration points used to construct the age model. **(a)** Summer (red) and Winter (blue) SST estimates from MAT and Mg/Ca SSTs (orange) plotted together; **(b)** *N. pachyderma* (s) coiling ratio (%); **(c)** Benthic (light blue) and planktonic (dark blue) $\delta^{18}O$ records of MD03-2664, plotted versus age (kyr BP). The black arrow indicate the onset of the cooling trend beginning at ~119 kyr BP, as inferred from the *N. pachyderma* (s) coiling ratio and the yellow vertical bar denotes the brief cooling event at ~117 kyr BP. (For interpretation of the references to colour in this figure legend, the reader is referred to the web version of this article.)

The benthic $\delta^{18}O$ record on the new age model is plotted on Fig. 3a together with benthic $\delta^{18}O$ record of MD95-2042 (Shackleton et al., 2000) and the LR04 benthic $\delta^{18}O$ stack (Lisiecki and Raymo, 2005).

According to our age model, mean sedimentation rates at site MD03-2664 range from ~34 cm/kyr over the MIS 5e plateau (128.0–116.1 kyr BP; corresponding to a mean temporal sample spacing of ~29 years/cm) to ~14 cm/kyr during MIS 5d (Fig. 3b). The large difference in sedimentation rates between the interglacial (MIS 5e) and stadial (MIS 5d) is expected given the local sedimentation regime (Hillaire-Marcel et al., 1994).

Following the age model approach used by e.g. Govin et al. (2012), we compared peaks in atmospheric methane recorded in ice cores to our records of North Atlantic SST in order to assess uncertainties in our age model for MD03-2664. The peak North Atlantic warmth (~127.7–127 kyr BP) at core MD03-2664 occur very close in timing to the early MIS 5e methane peak (~128.6–127.6 kyr BP) (on EDC3 chronology, Parrenin et al., 2007)—suggesting the MD03-2664 age model is also consistent with the EDC3 chronology to within some hundreds of years.

The benthic $\delta^{18}O$ stratigraphies from the subpolar North Atlantic sites ODP 980 and NEAP-18K, and site HM57-7 from the Iceland Sea are plotted versus age in Fig. 7e. We facilitate a comparison with proxy records from these sites by placing their results on a common timescale. We use the benthic $\delta^{18}O$ plateau (128 and 116.1 kyr BP) to assign ages following Shackleton et al. (2002, 2003), and use IRD records and assign additional tie points for the H11 (131 kyr BP) and C24 (111 kyr) events. It is important to note that offsets of up to a few thousand years are possible

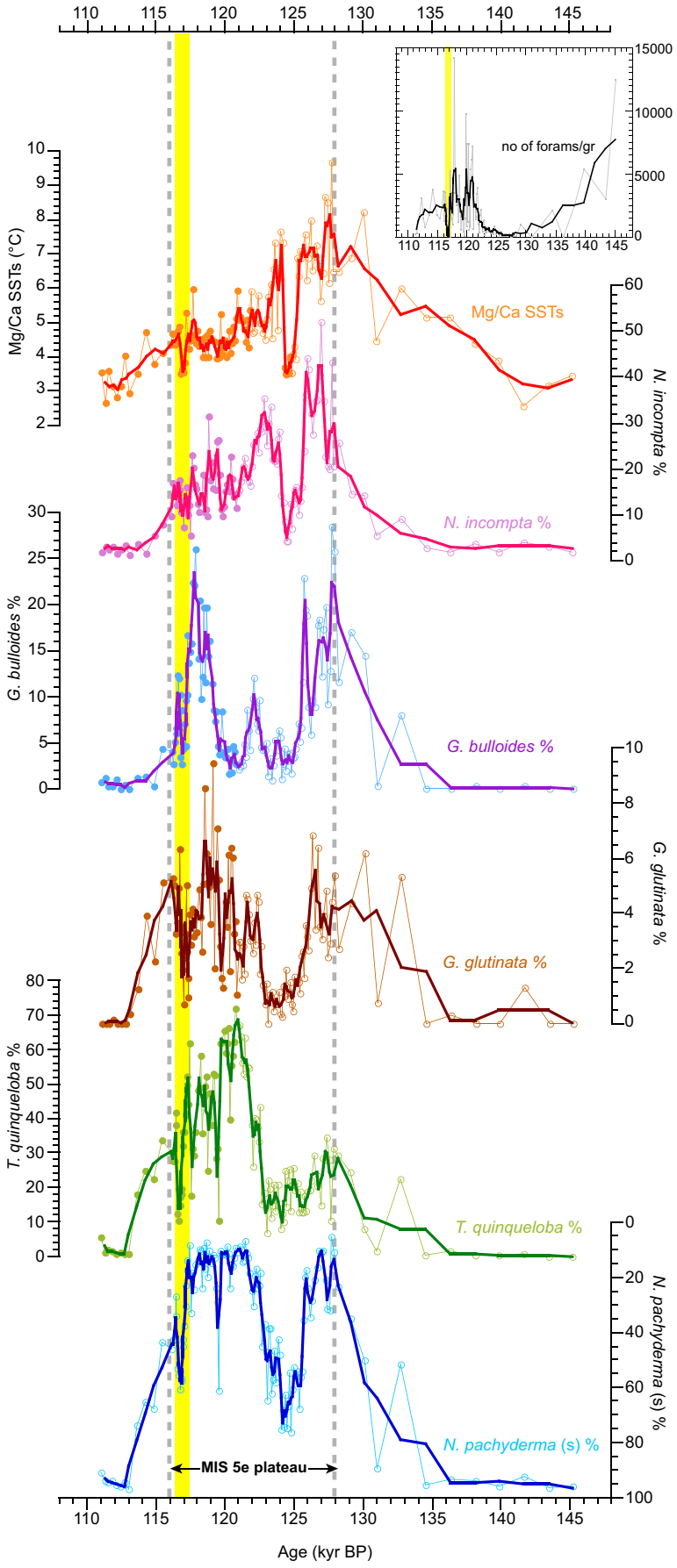

Fig. 6. Mg/Ca SSTs and the relative abundances of *N. incompta*, *G. bulloides*, *G. glutinata*, *T. quinqueloba* and *N. pachyderma* (s) plotted versus age (kyr BP), with a 3-point running mean (bold line). The dashed vertical lines denote the MIS 5e benthic $\delta^{18}O$ plateau. Open circles mark the previously published MD03-2664 data (Galaasen et al., 2014; Irvalı et al., 2012), whereas filled circles mark new data. Inset shows the number of foraminifera/per gram sediment, with a 5-point running mean (black line). Yellow bands mark the 117 kyr BP cooling event.

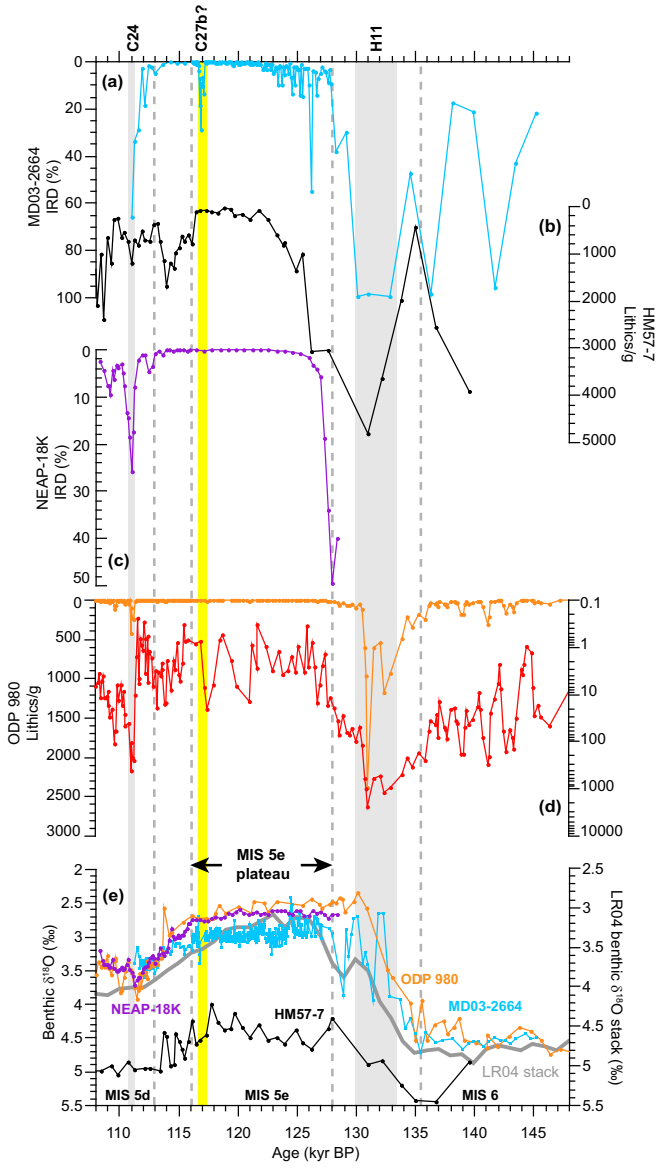

Fig. 7. Comparison of IRD records **(a)** MD03-2664 (green); **(b)** HM57-7 (black); **(c)** NEAP-18K (purple); **(d)** ODP 980 (orange in linear and red in logarithmic scale); **(e)** Comparison between benthic oxygen isotope records of MD03-2664 (light blue), HM57-7 (black), NEAP-18K (purple) and ODP 980 (orange), plotted versus age model used for the MD03-2664, based on Shackleton et al. (2002, 2003). The dashed vertical lines denote the calibration points used to construct the age model. (For interpretation of the references to colour in this figure legend, the reader is referred to the web version of this article.)

between benthic $\delta^{18}O$ records from different oceans, hemispheres, and water masses (e.g., Govin et al., 2012; Skinner and Shackleton, 2005). However, here we tie records from sites that have well-defined isotope plateaus and large-scale events (H11, C24). In addition, today all sites are influenced by (proto) North Atlantic Deep Water (NADW). Based on this rationale, the sites should experience similar benthic $\delta^{18}O$ evolutions through time—minimizing the potential offsets associated with this approach. In Fig. 7e, we also show the LR04 benthic $\delta^{18}O$ stack (Lisiecki and Raymo, 2005) as a common stratigraphic reference that is used by many investigators in order to illustrate the similarity between the LR04 stack and our synchronized records.

5. Results

5.1. Ice-rafted debris (IRD) and N. pachyderma (s) relative abundance

IRD abundance is high and variable during the late MIS 6, fluctuating between 17% and 98% (Fig. 4). Towards the end of MIS 6, IRD increases up to 99.5% marking an event of massive iceberg discharge, associated with H11. The relative abundance of polar planktonic foraminifera *N. pachyderma* (s) % is high (>95%) and remains stable through late MIS 6. Prior to H11, *N. pachyderma* (s) % drop to ~50%, but increases to 90% at the mid point of the IRD maxima at H11. By the onset of the MIS 5e benthic $\delta^{18}O$ plateau, at 128 kyr BP, IRD % and the relative abundance of *N. pachyderma* (s) decrease from 98 to 9% and 90 to 11%, respectively. During the early part of MIS 5e, between 128 and 122 kyr BP, small amounts of IRD (10–15%) continue to be present. IRD nearly disappears at 122 kyr BP, shortly after the end of the cooling event between ~126 and 124 kyr BP (Irvalı et al., 2012), which is marked by increased abundance of the polar planktonic foraminifer *N. pachyderma* (s). The abundance of IRD remains near-zero (Fig. 4a), from ~122 to 117 kyr BP suggesting that, despite its proximity to Greenland, no icebergs were supplied, and/or survived transport to our core site during this time period.

Towards the end of the benthic $\delta^{18}O$ plateau at ~117.1 kyr BP, IRD % increase from zero to 14% and reach a maximum of 29% at ~116.9 kyr BP. Coeval with the IRD increase, the relative abundance of *N. pachyderma* (s) increases to 61% and dominates the foraminiferal assemblage suggesting cold, iceberg laden waters invaded the site at this time. This late MIS 5e cold episode, centered at ~117 kyr BP, is the first event where IRD increases to greater than 5% since early MIS 5e and the waning stages of MIS 6, suggesting that the GIS had once again grown to a size where significant icebergs were generated and survived transport to the study area. This is consistent with a general climate cooling and the less intense summers that immediately preceded the ~117 kyr BP event, indicated by the steady increase in *N. pachyderma* (s) % (Fig. 4c) and MAT SST decrease (Fig. 5), which may have promoted or occurred in response to ice sheet build up prior to this event.

Following the ~117 kyr BP cooling event, IRD % drops back to near zero values. *N. pachyderma* (s) % also decreases to 27%. This recovery is brief, lasting ~400 years before the onset of the MIS 5e/5d transition. *N. pachyderma* (s) abundance reaches 97% by 113 kyr BP, at the onset of MIS 5d. Despite the gradually increasing trend in the *N. pachyderma* (s) % record, IRD % remains low throughout the MIS 5e/5d transition between 116.5 and 113 kyr BP, before increasing again in a stepwise manner after 113 kyr BP and reaching a maximum of 65% at 111 kyr BP. This IRD event is most likely the local equivalent of the widely observed C24 event which occurs at the peak of MIS 5d (Hodell et al., 2009; McManus et al., 1994).

Consistent with previous studies (e.g., McManus et al., 1994), each increase in IRD% is associated with an increase in the relative abundance of polar planktonic foraminifera *N. pachyderma* (s), however not all increases in *N. pachyderma* (s) % are accompanied by increases in IRD%. This suggests that polar conditions occurred in conjunction with the arrival of debris-laden icebergs, but increased influence of polar waters alone were not necessarily sufficient to increase IRD. Hence, similar *N. pachyderma* (s) % changes have different IRD signatures. For instance, the similarity in relative abundance of *N. pachyderma* (s) % during cold events at ~119.5 kyr BP (62%) and ~117 kyr BP (61%) suggests broadly similar surface ocean conditions. However, despite the similar increase in *N. pachyderma* (s) relative abundance, the 119.5 kyr BP cooling is associated with only trace amounts of IRD (1.5%), whereas IRD increases up to 29% at ~117 kyr BP (Fig. 4c). Clearly the relationship is

not linear and also depends on the boundary conditions, for example when the ice sheet is relatively large the response will be greater. In effect, changes in ice sheet size and/or the rate of iceberg supply must also have occurred.

5.2. Planktonic foraminiferal assemblages and sea surface temperatures

SSTs at Eirik Drift reach peak values during early MIS 5e, between 128 and 126 kyr BP. This is shown both by Mg/Ca and MAT derived SSTs (Fig. 5a), as well as high abundances of subpolar to transitional planktonic foraminifer species (e.g., *N. incompta*, *G. bulloides*, *G. glutinata*) at the site (Fig. 6). *N. incompta* reaches its maximum abundance during early MIS 5e, forming up to 52% of the total assemblage, whereas the abundance of *T. quinqueloba* and *N. pachyderma* (s) are generally below 30%. Compared with modern Mg/Ca and MAT SSTs reconstructed from a nearby core-top (Kleiven et al., 2010), SSTs during early MIS 5e reflect 2–5 °C warmer than present conditions (core top values shown in Irvalı et al., 2012 Fig. 4). The early MIS 5e SST maximum indicated by MAT are, within error, at least as high as those achieved during the entire of the interglacial suggesting peak warmth was achieved early in MIS 5e.

Polar water influence increased at our site at ~126 kyr BP, as the foraminiferal assemblage shifts from subpolar *N. incompta* (decreasing from 44% to 4.5%) to polar *N. pachyderma* (s) (increasing from 18% to 76%) dominance. MAT SSTs indicate a cooling of ~3 °C and ~3.3 °C during summer and winter, respectively. Likewise, Mg/Ca SSTs decrease by ~3.4 °C during the cooling event. Compared to our previously published Mg/Ca record (Irvalı et al., 2012), the duration of the 126 kyr BP cooling event is now better resolved with the addition of new data points during this interval, suggesting a similar magnitude and duration (~1 kyr) in all SST records (i.e., Mg/Ca and MAT derived). This cooling is also associated with an abrupt ~0.8‰ decrease in *N. pachyderma* (s) $\delta^{18}O$, which occurs over 4 cm (~120 years) (Fig. 3). The decrease in $\delta^{18}O_{sw}$ implies fresher near surface conditions at this time. This freshening/cooling event spans the period of most intense intra-MIS 5e deep water ventilation reductions inferred from benthic $\delta^{13}C$ records (i.e., Galaasen et al., 2014). Lowest *G. bulloides* % and *G. glutinata* % (Fig. 6) during these intervals of increased polar (cold/fresh) water influence suggest lower productivity during these intervals. Hence productivity related influences on the benthic $\delta^{13}C$ records (Mackensen et al., 1993) are most likely minimal; consistent with the interpretation that deep water ventilation changed at this time (Galaasen et al., 2014).

During mid-MIS 5e, beginning approximately at 122.8 kyr BP, SSTs (both Mg/Ca and MAT), *N. incompta* % and the *N. pachyderma* (s) coiling ratio starts to decrease gradually, with a sharper decline occurring at ~122 kyr BP (Figs. 5 and 6). Coincident with this shift, *T. quinqueloba* % starts to increase at ~122.5 kyr BP and reaches its maximum abundance (72%) at ~121 kyr BP (Fig. 6), most likely indicating a very proximal Arctic Front to our site at this time. Another cooling event occurs centered at ~119.5 kyr BP, also indicated by an increase in *N. pachyderma* (s) % abundance. Following the cooling at ~119.5 kyr BP, MAT summer and winter SSTs increase immediately, indicating a warming between 119.5 and 117.5 kyr BP, while the Mg/Ca SSTs remain low and increase to MAT winter SST levels again at ~118 kyr BP. Although *T. quinqueloba* % remains relatively high from 122.5 to 117 kyr BP, fluctuations between high relative abundances of *T. quinqueloba* % and *N. pachyderma* (s) % (and vice versa) occur, (e.g., at 119.5 kyr BP, *T. quinqueloba* % decreases from 62 to 11% while *N. pachyderma* (s) % increases from 10 to 62%), and this reverse relationship might reflect the repeated advances and retreats of Arctic and Polar fronts relative to our core site.

Our results show that the region south of Greenland began cooling prior to the end of the MIS 5e benthic $\delta^{18}O$ plateau. Following the recovery of the cooling recorded at ~119.5 kyr BP, reconstructed MAT winter SSTs and the % of sinistral coiling *N. pachyderma*, which thrive in cool waters (≤7 °C; Tolderlund and Bé, 1971), begin to decrease/increase respectively at ~119 kyr BP—a few thousand years prior to the end of the benthic $\delta^{18}O$ plateau (116.1 kyr BP) (Fig. 5). This suggests that regional surface water cooling, at least during winter and spring, began prior to major continental ice sheet growth and/or bottom water cooling at our site. The trend toward cooler surface conditions is most evident in the coiling ratio of *N. pachyderma* (s) % (Fig. 5b), which shifts rapidly and nearly monotonically from less than 40% to over 55% between 119.0 and 117.5 kyr BP. This trend is interrupted by a distinct ~400 year long episode of even colder conditions centered at ~117 kyr BP. During this cooling, the coiling ratio (%) of cryophilic *N. pachyderma* (s) rises to 86% while the *N. pachyderma* (s) $\delta^{18}O$ increases by ~0.9‰ to MIS 5d-like absolute values of ~3.5‰. This event lasts ~400 years on our age model, but is difficult to determine precisely without independent age constraints within this interval. Indeed, a higher sedimentation rate at this time is possible. A decrease in foraminifera to total sediment ratio (Fig. 6) suggests that biogenic components may have been diluted by an increase in non-biogenic fine fraction sediment sources during the 117 kyr BP event. Although *C. wuellerstorfi* were not continuously present through this interval, benthic $\delta^{18}O$ values of approximately 3.0‰ recorded within the cooling interval are typical of mean MIS 5e benthic $\delta^{18}O$ values (Fig. 5c)—suggesting no considerable change in bottom water physical properties (or sand-size sediment remobilization) at this time.

Small changes are also registered in SSTs during the ~117 kyr BP event. Mg/Ca SSTs decrease from 5.3 °C to 3.6 °C – indicating a cooling of ~1.7 °C. Summer and winter coolings of ~1.7 °C and ~2.2 °C are indicated from the MAT results; summer SSTs decrease from 9.8 ± 0.8 °C to 8.1 ± 0.8 °C, while winter SSTs decrease from 5.7 ± 0.7 °C to 3.5 ± 0.9 °C. Although the dissimilarity coefficient is low (<0.1) through the cooling event, the standard deviation is relatively high (up to 1.8 °C) for a few samples (Fig. 2e and f), most likely due to high percentages of *N. pachyderma* (s). According to core-top assemblages, the relationship between *N. pachyderma* (s) abundances and SST weakens when the former approaches 100%, as this may correspond to a wide range of temperatures (Kohfeld et al., 1996; Oppo et al., 2006; Prell et al., 1999).

The fact that the 117 kyr BP event registers more strongly in the *N. pachyderma* (s)-based proxies (i.e., % and $\delta^{18}O$) suggests that the cooling was stronger in the calcifying environment of this species—most likely during the spring or summer bloom season (Tolderlund and Bé, 1971). The clear increase in coiling ratio of *N. pachyderma* (s) after 119 kyr BP suggests a steady decline in SSTs persisting into the time of spring bloom when light and food are available to support larger numbers of *N. pachyderma* (s) at the expense of less cold-adapted species.

Increasing numbers of polar foraminifera and decreasing MAT SSTs suggest that gradual cooling continued at Eirik Drift after the recovery of the 117 kyr BP event. Between 116.1 and 113.6 kyr BP MAT Summer and Winter SSTs decline gradually by ~1.3 °C and 1.8 °C, respectively. This is followed by a sharper decline of 5.6 °C and 3.8 °C at ~113 kyr BP—coeval with a rapid ~0.4‰ increase in *N. pachyderma* (s) $\delta^{18}O$ at the final transition to full MIS 5d conditions. This general progression of gradual/modest cooling followed by larger/more rapid cooling during the MIS 5e/5d transition is similar to the pattern found in the Greenland ice cores (i.e., NGRIP, NEEM) (Landais et al., 2006; NEEM community members, 2013) and high resolution sites in the subpolar North Atlantic (i.e., ODP 980; Oppo et al., 2006). Oppo et al. (2006) argued that this sharp

cooling marked the end of interglacial warmth in many regions, including the circum-Atlantic, the central subpolar North Atlantic (Chapman and Shackleton, 1999), west Iberia and southern Europe (Sánchez Goñi et al., 2005) and the western subtropical Atlantic (Lehman et al., 2002; Oppo et al., 2001). In summary, there is evidence for regional multi-season cooling commencing with the initiation of major continental ice growth and/or bottom water cooling (benthic $\delta^{18}O$ increase) associated with the sharp transition to MIS 5d conditions with surface waters approximately 6 °C cooler than during the preceding MIS 5e conditions.

6. Discussion

Our new high-resolution multi-proxy records from the Eirik Drift add to a growing body of evidence for North Atlantic climate and ice sheet variability during the last interglacial period (e.g., Bauch et al., 2011; Bond et al., 2001; Fronval and Jansen, 1997; Hibbert et al., 2010; McManus et al., 1994; Oppo et al., 2006) and expands the spatial distribution of available sites for depicting the progression of North Atlantic climate, ocean frontal positions, and ice sheet variability during MIS 5e. Here we compare these new proximal Greenland records with existing records from the eastern subpolar North Atlantic (ODP site 980; Oppo et al., 2006), central subpolar North Atlantic (core NEAP-18K; Chapman and Shackleton, 1999) and the Nordic/Iceland Sea (core HM57-7; Fronval and Jansen, 1997) (Fig. 7)—refining our picture of regional IRD-climate patterns and further elucidating the behavior of the GIS during the peak last interglacial period (MIS 5e). In addition, we utilize the information provided by the foraminiferal assemblages to provide new insights into spatio-temporal evolution of frontal positions (Polar and Arctic Fronts). By adding a site close to the modern fronts' position we can identify even moderate southward advances and better characterize the onset of cooling phases (Fig. 9).

6.1. Comparison with other IRD records and ice sheet variability

IRD input south of Greenland shows similarities with North Atlantic and particularly Nordic Seas records from late MIS 6 into early MIS 5e. High and variable IRD input characterizes late MIS 6 and Termination II at all sites studied (Fig. 7). In the central (NEAP-18K) and eastern subpolar North Atlantic (ODP 980) IRD % decreases to near-zero values immediately following the H11 event and only trace amounts of IRD are present at ODP Site 980 during early MIS 5e (Oppo et al., 2006)—indicating that few icebergs survived transport to these sites. The IRD record from the Iceland Sea (HM57-7) bears particularly strong resemblance to the Eirik Drift record following the initiation of the MIS 5e benthic $\delta^{18}O$ plateau. In contrast to the sharp reduction in IRD observed in the central and eastern North Atlantic sites at the beginning of MIS 5e, IRD abundance decreases more gradually in the Iceland Sea (Fronval and Jansen, 1997). South of Greenland, IRD also tapers off gradually during the first part of the MIS 5e benthic $\delta^{18}O$ plateau, with small amounts of IRD present until ~122 kyr BP when IRD % decreases to near-zero. Taken together, the pattern suggests that icebergs (and detritus rafting) persisted in significant amounts in the colder regions proximal to Greenland well into the beginning of MIS 5e while more distal sites in the North Atlantic and Nordic Seas received little or no IRD input, as the Polar Front was shifting northeast from its southernmost position at MIS 6. Thus, the steady decline in IRD % recorded at our core site during early MIS 5e likely represents a persisting input of IRD from East Greenland tidewater glaciers, in pulses of decreasing size, as this is the most proximal source of icebergs found in our site and Iceland Sea records. The lack of IRD after ~122 kyr BP suggests that few icebergs were supplied or survived transport to our site by mid MIS 5e, i.e., GIS

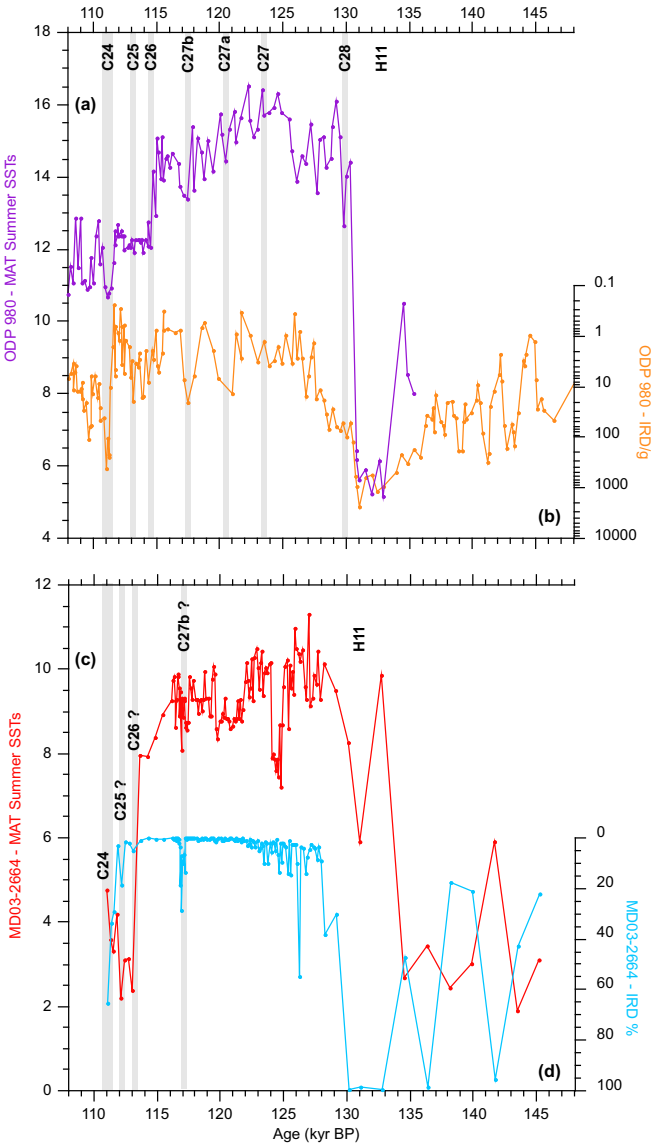

Fig. 8. Comparison of ODP 980 and MD03-2664 MAT Summer SSTs and IRD records over the MIS 5e: **(a)** ODP 980 MAT Summer SST record (purple); **(b)** ODP 980 IRD/g record on logarithmic scale (orange); **(c)** MD03-2664 MAT Summer SST record (red) **(d)** MD03-2664 IRD% record (blue). C events on (a) and (b) are marked after Oppo et al. (2006). (For interpretation of the references to colour in this figure legend, the reader is referred to the web version of this article.)

was largely terminating inland, similar to the situation during the mid-Holocene (e.g., Funder et al., 2011).

Decrease in iceberg supply due to a diminishing GIS extent is the most likely reason for the trend toward lower IRD % at our site—at least until after ~126 kyr BP when local surface water cooling (Fig. 5) should have once again promoted iceberg survival, as the influence of polar waters increased off south of Greenland. Pollen and sediment chemistry studies on the extent of GIS (Carlson et al., 2008; Colville et al., 2011; de Vernal and Hillaire-Marcel, 2008) also suggest a rapid retreat of the ice sheet during early MIS 5e. Seen in this way, the pulsed nature of the IRD input is interesting and may reflect surging or collapses of the GIS as it wasted. Records with equivalent resolution located more proximal to the main sources of IRD in east Greenland would be useful for testing/confirming this hypothesis.

Similar to records from both the North Atlantic (Chapman and

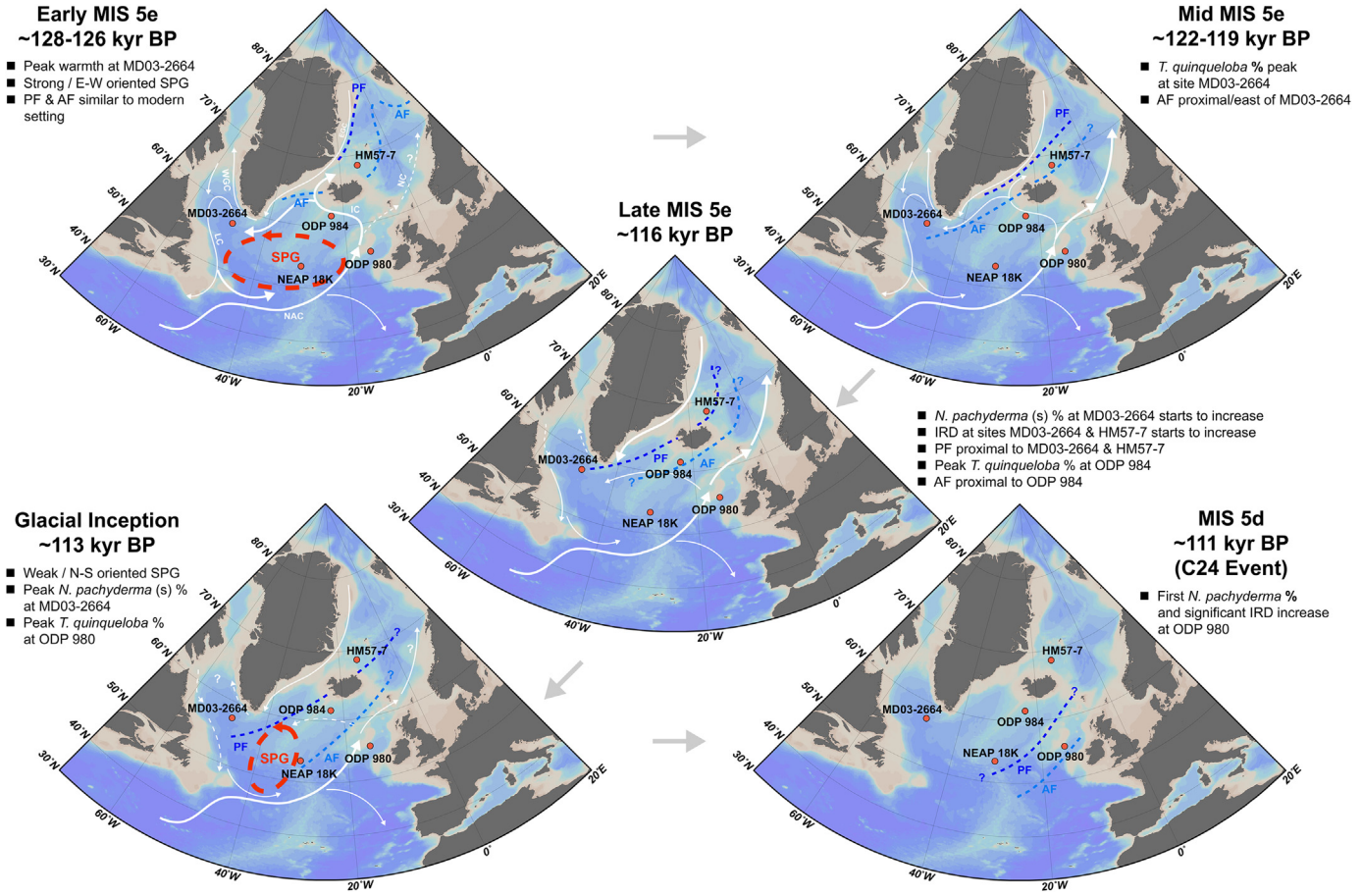

Fig. 9. Schematic representation showing the evolution of surface hydrography and frontal positions during different phases of MIS 5e and MIS 5d. Red circles mark the location of core sites mentioned in the discussion: MD03-2664 (this study), ODP Site 980 (Oppo et al., 2006), ODP Site 984 (Mokeddem et al., 2014), NEAP-18K (Chapman and Shackleton, 1999), and HM57-7 (Fronval and Jansen, 1997). PF: Polar Front, AF: Arctic Front. (For interpretation of the references to colour in this figure legend, the reader is referred to the web version of this article.)

Shackleton, 1999; Oppo et al., 2006) and the Nordic Seas (Bauch et al., 2011; Fronval and Jansen, 1997), IRD is present but in relatively minor amounts during mid MIS 5e, indicating minimal calving of tidewater glaciers and distal iceberg transport. Our SST estimates suggest that this period of low IRD % is associated with relatively warm SSTs south of Greenland (Figs. 4 and 5), consistent with a period of reduced GIS extent or iceberg transport/survival to the core site from ~122 to 119 kyr BP. This is also in agreement with high spore and pollen concentrations south of Greenland during this interval, and indicates expansion of vegetation on Greenland and ice extent minimum (de Vernal and Hillaire-Marcel, 2008).

Faunal and SST proxies indicate a trend toward colder and more polar-like surface waters south of Greenland beginning at ~119 kyr BP (Figs. 5 and 6). This gradual cooling trend leading up to the MIS 5e/5d transition was interrupted by a transient cooling event centered at 117 kyr BP. A late MIS 5e cooling event has also been documented in the central and eastern subpolar North Atlantic (Chapman and Shackleton, 1999; Mokeddem et al., 2014; Oppo et al., 2006). A similar pattern of gradual cooling interrupted by an abrupt cooling event before the end of MIS 5e benthic $\delta^{18}O$ plateau, is also observed in the eastern subpolar North Atlantic (ODP 980). This cooling event was labeled "C27b" by Oppo et al. (2006). At ODP Site 980, this event is associated with trace amounts of IRD and is followed by a short warming/recovery before the sharper cooling that marks the C26 cooling and the glacial inception at this site (Fig. 8). Since the large cooling associated with the C26 event occurs after the end of the "MIS 5e benthic $\delta^{18}O$ plateau" (i.e., occurs after the sea level has begun to drop significantly) and marks the end of MIS 5e in previous records from subpolar North Atlantic (Mokeddem et al., 2014; Oppo et al., 2006), to central North Atlantic (Chapman and Shackleton, 1999) and through western subtropical Atlantic (Lehman et al., 2002) we suggest that the 117 kyr BP cooling (which occurs prior to the end of MIS 5e benthic $\delta^{18}O$ plateau) at the Eirik Drift should be earlier than the C26 event. Hence, based on comparison with other SST records and its timing clearly within the MIS 5e plateau we suggest that our 117 kyr event is most similar to the C27b event as identified by Oppo et al. (2006).

South of Iceland (ODP Site 984) the C27b cooling event is marked by decreased *N. incompta* (*N. pachyderma* (d)) abundance (Mokeddem et al., 2014). Likewise, a cooling is recorded by an increase (~0.4‰) in planktonic $\delta^{18}O$ values in core NEAP-18K from the central subpolar North Atlantic (Chapman and Shackleton, 1999), and by Greece pollen records (Milner et al., 2013). Each of these regional cooling events occurred late in MIS 5e (before the end of MIS 5e plateau) and may represent a synchronous cooling event. Regardless of whether they are contemporaneous, they suggest that climate variability increased as North Atlantic summer insolation reached its nadir and surface waters began to cool towards the end of MIS 5e.

The magnitude of the abrupt increase in the *N. pachyderma* (s) $\delta^{18}O$ record during the 117 kyr event at site MD03-2664 (~0.9‰) is

similar in magnitude to the $\delta^{18}O$ shift during the MIS 5e/5d transition. The rate and duration of the event suggests that it involved a rapid shift in the North Atlantic Ocean circulation. In a recent study Hansen et al. (2016) mark the similarity in duration of the 117 kyr cooling event (~400 years) to a cold-stormy period (468 years) as observed from German lake sediment records (Sirocko et al., 2005), which has been related to southward shift of the polar front; consistent with a southward advance of colder polar waters observed at our site. The spatial extent and expression of this anomaly suggests it involved a rapid and large-scale shift in North Atlantic ocean-atmospheric circulation patterns; in some locations approaching the scale of changes that mark the MIS 5e/5d transition. Yet, unlike the onset of glaciation it was temporary and did not involve the large changes (increases) in continental ice sheets. A single low benthic $\delta^{13}C$ point during the 117 kyr event at site MD03-2664 (Galaasen et al., 2014) hints that the surface cooling may have been accompanied by a reduction in the deep ocean ventilation rate (e.g. reduced NADW) and additional data portraying deep circulation should be prioritized to confirm that this event was coupled to a change in thermohaline circulation.

At the Eirik drift, the 117 kyr BP cooling event is associated with the first significant increase in IRD % since the waning stages of MIS 6 and early MIS 5e. A similar increase in IRD prior to the end of the MIS 5e benthic $\delta^{18}O$ plateau has also been found in the Nordic Seas (Bauch et al., 2011; Fronval and Jansen, 1997) (Fig. 7). Despite clear evidence for cooling episodes in the central and eastern subpolar North Atlantic during the C27b event late in MIS 5e (Chapman and Shackleton, 1999; Mokeddem et al., 2014; Oppo et al., 2006), only trace amounts of IRD are found in these regions. Indeed, the first significant IRD increases in both the central and eastern subpolar North Atlantic occur well after the end of the MIS 5e benthic $\delta^{18}O$ plateau, during early MIS 5d (the C25 event) in central subpolar Atlantic records (NEAP-18K), and during late MIS 5d (the C24 event) in the eastern subpolar North Atlantic (ODP 980) (Chapman and Shackleton, 1999; Mokeddem et al., 2014; Oppo et al., 2006). Thus, the spatial pattern of late MIS 5e IRD increases mirrors the pattern of early MIS 5e decrease, with greater amounts of IRD in the Nordic Seas and Eirik Drift (south Greenland) records than in the North Atlantic during both the waxing and waning stages of MIS 5e.

The late MIS 5e IRD increase in proximal Greenland records suggests that regional ice sheets and tidewater glaciers had begun to expand prior to the end of the MIS 5e benthic $\delta^{18}O$ plateau, likely related to reduced summer insolation (Laskar et al., 2004) perhaps reinforced by expansion of polar waters and surface cooling after ~119 kyr BP (Fig. 5). The source of ice-rafted grains to the Nordic Seas are the surrounding continental land masses, primarily Greenland, Iceland, and Fennoscandinavia (e.g., Elliot et al., 1998), with the GIS being the major IRD source for the Iceland Sea (Bischof, 1994; Fronval and Jansen, 1997; Fronval et al., 1995). The pattern of IRD increases points toward a relatively early regrowth of the GIS within MIS 5e. In the Nordic Seas records, IRD concentrations increase the most in records closest to Greenland (e.g., HM57-7 in the Iceland Sea; Fronval and Jansen, 1997). Given the proximity of MD03-2664 and HM57-7 to Greenland, IRD flux at both sites should primarily reflect fluctuations in the GIS. Taken together, this suggests that the GIS was growing as regional SSTs were dropping prior to the onset of major continental glaciation (as indicated by benthic $\delta^{18}O$ increase at the MIS 5e/d transition).

Our identification of a strong cooling and increased IRD % at 117 kyr BP likely marks the period when a significant amount of ice had repopulated Greenland. The ~117 kyr BP cooling most likely corresponds to the interval when pollen and spore concentrations south of Greenland had considerably decreased towards the end of MIS 5e (de Vernal and Hillaire-Marcel, 2008) and to the interval with reduced GIS ablation based on [Ti] and [Fe] records (Carlson et al., 2008) indicating regional cooling and the onset of ice growth before the end of MIS 5e benthic $\delta^{18}O$ plateau. In agreement, the NEEM ice core records suggest Greenland itself started a long-term cooling extending into MIS 5d prior to this event at ~120 kyr BP (NEEM community members, 2013).

6.2. Evolution of sea surface hydrography and fronts

With the initiation of MIS 5e benthic $\delta^{18}O$ plateau, SSTs at the Eirik Drift reached peak values. Low abundances of *N. pachyderma (s)* % and *T. quinqueloba* % at site MD03-2664 during this warmest interval suggests that the Arctic Front was probably further north relative to our core site and that Atlantic/Irminger Current (IC) waters were the main influence south of Greenland. Early peak MIS 5e warmth at Eirik Drift suggests increased contribution of IC (relative to EGC) at our site (Irvalı et al., 2012)—indicating a stronger SPG circulation during early MIS 5e (as opposed to a weak SPG circulation recently suggested by Mokeddem et al. (2014) for the early MIS 5e). A stronger and more E-W oriented SPG early in MIS 5e would transport more warm and saline waters of subtropical origin to the vicinity of our study area as opposed to the Nordic Seas, and could explain the delayed MIS 5e peak warmth observed in the records from eastern Nordic Seas (e.g., Rasmussen et al., 2003; Van Nieuwenhove et al., 2013; Van Nieuwenhove et al., 2011). Peak warmth in early MIS 5e is consistent with the NEEM ice core records (NEEM community members, 2013) and model findings (Bakker et al., 2013, 2014; Capron et al., 2014; Govin et al., 2012; Otto-Bliesner et al., 2006), but at odds with some previous inferences based on lower resolution single proxy records (e.g., Govin et al., 2012). This early peak warmth occurred despite a potentially reduced deep water production at this time (e.g., Hodell et al., 2009). Indeed, our records suggest that it was only during the transient reduction in NADW between 126 and 124 kyr BP (Galaasen et al., 2014) that SSTs south of Greenland decreased. This scenario is quite different than previous studies, which suggest freshwater input, potentially from melting Northern Hemisphere ice sheets, delayed the onset of deep water production and peak warmth. Our Eirik Drift records confirm that full, if not peak, warmth was achieved early as was near modern deep water production (Galaasen et al., 2014), and was only interrupted by brief cooling intervals in MIS 5e associated with transient reductions in NADW influence (Galaasen et al., 2014). Because the largest of these cool episodes occur early in MIS 5e, just after peak warmth is achieved, lower resolved records may smooth (or miss entirely) the periods of early MIS 5e warmth with the periods of cooler SSTs that occur just before and after them, resulting in an aliased picture of MIS 5e SST evolution (i.e., giving the appearance of delayed warming).

During mid-MIS 5e, between 122 and 119 kyr BP, high *T. quinqueloba* % abundance at site MD03-2664 suggests that the Arctic Front was proximal to our site. This is slightly earlier than the *T. quinqueloba* % peaks recorded at Sites ODP 984 (Mokeddem et al., 2014) and ODP 980 (Oppo et al., 2006), which reach peak percentages just before the end of MIS 5e benthic plateau and after the end of MIS 5e benthic plateau, respectively. This delayed *T. quinqueloba* % increase towards the southern sites would therefore suggest a gradual southward advance of the Arctic Front starting at ~122.5 kyr BP at south of Greenland (MD03-2664), then reaching south of Iceland (ODP 984) before the end of MIS 5e, and finally reaching to the eastern subpolar North Atlantic (ODP 980) by the onset of MIS 5d, at ~113 kyr BP.

During late MIS 5e, following the gradual cooling trend after ~119 kyr BP, the Polar Front advanced south. Nordic Seas and south Greenland records were more proximal to the Polar Front, which allowed icebergs to survive transport to our site during the 117 kyr

BP cooling event, while the position of the Arctic Front was still west of/proximal to south of Iceland at this time. The decrease in *G. bulloides* and *G. glutinata* abundances during the 117 kyr BP cooling event and the glacial inception most likely indicates less food source due to sea ice expansion and/or proximity to the Polar Front.

Compared to the eastern subpolar North Atlantic (ODP Site 980) record, SST records from south of Greenland (MD03-2664) indicate a greater cooling at the end of the MIS 5e (Fig. 8). For example, MAT Summer SSTs at site MD03-2664 shows a sharp decrease of ~5.6 °C at 113 kyr BP, whereas MAT Summer SSTs at ODP Site 980 decrease by ~3 °C at the end of MIS 5e, and decrease another ~2 °C during the C24 event, taking an additional ~2 kyr to reach the same magnitude of cooling observed at site MD03-2664. Similarly the polar *N. pachyderma* (s) % at site MD03-2664 reach 97% at 113 kyr BP, immediately after the onset of MIS 5d, whereas the first significant *N. pachyderma* (s) % increase south of Iceland (ODP Site 984) occurs slightly later in early MIS 5d (during the C25 event), and in the eastern subpolar North Atlantic (ODP Site 980) during late MIS 5d (during the C24 event). The Polar Front was probably already south of site MD03-2664 during the glacial inception at ~113 kyr BP (peak *N. pachyderma* (s) %), and reached ODP Site 984 by the C25 cooling during early MIS 5d (first significant *N. pachyderma* (s) % increase). Meanwhile, the Arctic Front was migrating south and was very proximal to ODP Site 980 at this time (peak *T. quinqueloba* %) (Fig. 9). The delayed response (increased IRD % & *T. quinqueloba* %) in southern sites (i.e., ODP Sites 984 and 980) may reflect their geographic distance from the Polar Front.

The increased influence of polar waters off south Greenland and the southward migration of the Polar Front after the end of MIS 5e could reflect a weaker and more contracted SPG circulation. The relative contribution of SPG waters into the Atlantic Inflow would decrease, allowing more warm and saline subtropical waters to enter the eastern subpolar North Atlantic and the Nordic Seas (Born et al., 2011), explaining the temperature gradient between the western (MD03-2664) and eastern (ODP Site 980) subpolar North Atlantic records during the onset of MIS 5d. Increased Atlantic Inflow and relatively warm conditions in the eastern subpolar North Atlantic and Nordic Seas during the glacial inception, despite a declining Northern Hemisphere summer insolation, is suggested by proxy and model data (Born et al., 2011; McManus et al., 2002; Mokeddem et al., 2014; Oppo et al., 2006), and postulated to provide a source of moisture by increasing the air-sea temperature contrast and help accelerate ice sheet growth (McManus et al., 2002). Alternatively, high SSTs may inhibit ice growth due to warming (Born et al., 2010a). Our proximal GIS records suggest ocean cooling is related to ice growth and may at least be critical for the ice sheet in achieving large, tide water calving glaciers. In their simulations Born et al. (2010b) suggest that Arctic sea ice played an important role during the glacial inception. They found that Arctic sea ice growth increased with the declining Northern Hemisphere summer insolation, allowing more sea ice to be transported south of the Greenland-Scotland Ridge through the EGC, which melted upon reaching the subpolar North Atlantic to affect the rim-to-center density contrast of and weaken the SPG (Born et al., 2010b). The weaker SPG resulted in less saline (IC) waters in the western North Atlantic which causes further relative freshening, while increasing the Atlantic Inflow into the Nordic Seas thus warming the region (Born et al., 2010a, 2010b). Our records are consistent with the weaker SPG pattern during the glacial inception, and the suggestion that sea ice as an important trigger for the initial weakening of the gyre before the onset of MIS 5d. Today the maximum sea ice edge is located west of the Arctic Front (Johannessen et al., 1994), and thus the southward migration of the fronts before the glacial inception, as inferred from our records, would have allowed sea ice to expand into lower latitudes. Sea ice expansions would further favor growth of continental ice sheets as SSTs decrease as a result of decreasing ocean-atmosphere heat flux and albedo feedbacks (Born et al., 2010b; Crucifix and Loutre, 2002).

Although early to respond, the new Eirik Drift records show that SSTs off Cape Farewell follow the typical North Atlantic progression from MIS 5e to MIS 5d with a similar pattern and magnitude to that observed in other high-resolution records (e.g., Oppo et al., 2006). Despite age uncertainties, the strong similarity in long-term temperature trends between the high-resolution subpolar North Atlantic SST records (i.e., MD03-2664, ODP Site 980) and the NEEM temperature record is interesting. Our SST records off south Greenland show a gradual cooling trend followed by a larger cooling event at ~119.5 kyr BP, followed by a warm interval between 119 and 117 kyr BP, gradual cooling beginning at ~119 kyr BP interrupted by a cooling event at ~117 kyr BP, a short recovery of 117 kyr BP cooling before the sharp decline into glacial inception—following a very similar evolution as the NEEM temperature change record (NEEM community members, 2013). Considering the scarcity of high-resolution SST records in proximity of the GIS spanning MIS 5e (e.g., Alley et al., 2010), our records may provide important constraints for modeling efforts attempting to resolve the sensitivity of climate and the GIS to MIS 5e forcing (e.g., Masson-Delmotte et al., 2011). Although the pattern of marine and ice core temperature changes is similar, the magnitude of inferred temperature changes over Greenland is much larger, supporting a role for elevation and/or seasonal moisture balance influencing Greenland ice core records (Masson-Delmotte et al., 2011; NEEM community members, 2013).

Finally, our records suggest that the overall glacial expansion

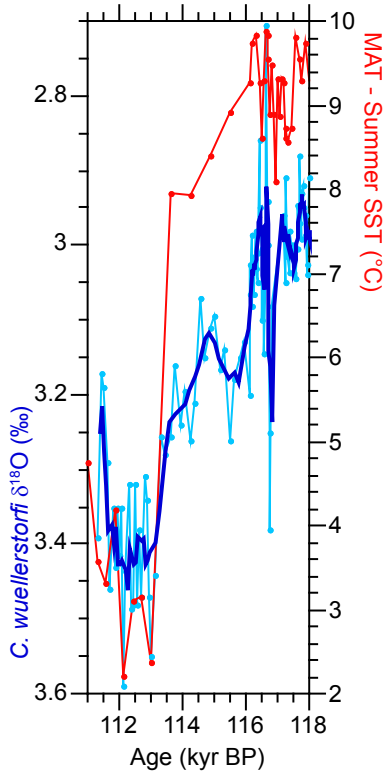

Fig. 10. Benthic $\delta^{18}O$ record (blue) plotted with a 5-point running mean and MAT Summer SSTs (red) are plotted together focusing over the glacial inception. (For interpretation of the references to colour in this figure legend, the reader is referred to the web version of this article.)

during inception (indicated by benthic $\delta^{18}O$) closely parallels the timing and pattern of SST evolution from MIS 5e to MIS 5d. Fig. 10 shows that MAT Summer SSTs and benthic $\delta^{18}O$ drop in parallel—benthic $\delta^{18}O$ begins to increase gradually when SSTs (all seasons) begin to decrease, and benthic $\delta^{18}O$ increase more sharply associated with the abrupt ~4 °C drop in SSTs. The pattern supports previous suggestions that ice sheets and North Atlantic climate are closely linked—either via the influence of ice sheets on climate (e.g., Clark et al., 1999) or that ocean cooling is a critical feedback for initiating large scale ice growth and inception (Khodri et al., 2001).

7. Summary and conclusions

Our new high-resolution records depict the evolution of surface ocean climate and IRD input south of Greenland through the peak of the last interglacial (MIS 5e) into the glacial inception. The IRD record indicates a tripartite structure in iceberg activity echoing the structure observed during the Holocene (Alley et al., 2010; Jennings et al., 2006). Significant IRD was present during early MIS 5e (benthic $\delta^{18}O$ plateau), tapering off gradually until approximately 122 kyr BP. The rapid decrease of tidewater glacial calving activity early in MIS 5e is consistent with the rapid wasting and retreat of the GIS at this time as inferred by other proxies (e.g., Carlson et al., 2008; Colville et al., 2011; de Vernal and Hillaire-Marcel, 2008) and found in models (e.g., Otto-Bliesner et al., 2006). During late MIS 5e our SST estimates indicate that the surface ocean began to cool with declining Northern Hemisphere summer insolation. Planktonic foraminiferal assemblages suggest a gradual southward advance of the Arctic Front starting at ~122.5 kyr BP off southern Greenland, and reaching the eastern subpolar North Atlantic by the onset of MIS 5d. Progressive advancement of fronts before the glacial inception and associated increases in Arctic sea ice could be an important trigger for weakening the SPG, and therefore the regional cooling and ice sheet growth before the onset of MIS 5d (e.g., Born et al., 2010b). Our results elucidate how the reconfiguration of the gyre and gyre dynamics may be critical for facilitating the sea ice expansion and demonstrate the potential importance of understanding the geographic structure of SST evolution through MIS 5e.

Following ~119 kyr BP our SST records show a gradual cooling trend which is interrupted by a brief episode of additional cooling (~117 kyr BP) and significant IRD input prior to the end of MIS 5e benthic $\delta^{18}O$ plateau and major glacial inception. This suggests that the GIS and tidewater glaciers increased late in MIS 5e as Northern Hemisphere insolation waned. Taken together the results are consistent with modeling studies suggesting significant changes in GIS extent and may help explain inferred changes in sea level within MIS 5e (Thompson et al., 2011; Thompson and Goldstein, 2006).

During inception, SSTs proximal to Greenland followed the progression previously observed in Greenland ice cores (Landais et al., 2006; NEEM community members, 2013) and across much of the North Atlantic and Europe—with modest/gradual cooling (~2 °C) from 116 to 114 kyr BP followed by stronger (~4 °C) and more abrupt cooling at ~113 kyr BP. The marine changes are however smaller than those observed in nearby Greenland (Landais et al., 2006; Masson-Delmotte et al., 2011), consistent with a role for amplifying feedbacks, such as ice sheet elevation or seasonal shifts in precipitation, on the Greenland ice core records (Masson-Delmotte et al., 2011; NEEM community members, 2013). Finally, the parallel evolution between climate and benthic $\delta^{18}O$ (global ice volume and deep ocean temperature) suggests a close coupling between the two-step inception and two-step cooling in North Atlantic climate.

Acknowledgments

The authors are grateful to IPEV, the captain and the crew of the *Marion Dufresne* and to the scientific party of the IMAGES P.I.C.A.S.S.O cruise. We also thank Dag Inge Blindheim and Rune Søraas at Uni Research for help with sample preparation and stable isotope analyses and Eva Bjørseth at Department of Earth Science for help with the map construction. This work is a contribution of the European Science Foundation EuroMARC program, through the AMOCINT project (grant number 187166), funded through grants from the Research Council of Norway, and RCN Frinatek project NOCWARM (grant number 205524), and contributes to EU-FP7 IP Past4Future. U. Ninnemann received funding for this study from a University of Bergen Meltzer research grant.

References

Alley, R.B., Andrews, J.T., Brigham-Grette, J., Clarke, G.K.C., Cuffey, K.M., Fitzpatrick, J.J., Funder, S., Marshall, S.J., Miller, G.H., Mitrovica, J.X., Muhs, D.R., Otto-Bliesner, B.L., Polyak, L., White, J.W.C., 2010. History of the Greenland ice sheet: paleoclimatic insights. Quat. Sci. Rev. 29, 1728–1756.

Alonso-Garcia, M., Sierro, F.J., Flores, J.A., 2011. Arctic front shifts in the subpolar North Atlantic during the Mid-Pleistocene (800-400 ka) and their implications for ocean circulation. Palaeogeogr. Palaeoclimatol. Palaeoecol. 311, 268–280.

Bacon, S., Reverdin, G., Rigor, I.G., Snaith, H.M., 2002. A freshwater jet on the east Greenland shelf. J. Geophys. Res. 107, 3068.

Bakker, P., Masson-Delmotte, V., Martrat, B., Charbit, S., Renssen, H., Gröger, M., Krebs-Kanzow, U., Lohmann, G., Lunt, D.J., Pfeiffer, M., Phipps, S.J., Prange, M., Ritz, S.P., Schulz, M., Stenni, B., Stone, E.J., Varma, V., 2014. Temperature trends during the Present and Last Interglacial periods – a multi-model-data comparison. Quat. Sci. Rev. 99, 224–243.

Bakker, P., Stone, E.J., Charbit, S., Gröger, M., Krebs-Kanzow, U., Ritz, S.P., Varma, V., Khon, V., Lunt, D.J., Mikolajewicz, U., Prange, M., Renssen, H., Schneider, B., Schulz, M., 2013. Last interglacial temperature evolution - a model inter-comparison. Clim. Past. 9, 605–619.

Bauch, D., Carstens, J., Wefer, G., 1997. Oxygen isotope composition of living Neogloboquadrina pachyderma (sin.) in the Arctic Ocean. Earth Planet. Sci. Lett. 146, 47–58.

Bauch, H.A., Kandiano, E.S., 2007. Evidence for early warming and cooling in North Atlantic surface waters during the last interglacial. Paleoceanography 22.

Bauch, H.A., Kandiano, E.S., Helmke, J., Andersen, N., Rosell-Mele, A., Erlenkeuser, H., 2011. Climatic bisection of the last interglacial warm period in the Polar North Atlantic. Quat. Sci. Rev. 30, 1813–1818.

Baumann, K.H., Lackschewitz, K.S., Mangerud, J., Spielhagen, R.F., Wolf-welling, T.C.W., Henrich, R., Kassens, H., 1995. Reflection of scandinavian ice sheet fluctuations in Norwegian sea sediments during the past 150,000 years. Quat. Res. 43, 185–197.

Bischof, J.F., 1994. The decay of the Barents ice sheet as documented in nordic seas ice-rafted debris. Mar. Geol. 117, 35–55.

Bond, G., Kromer, B., Beer, J., Muscheler, R., Evans, M.N., Showers, W., Sharon, H., Lotti-Bond, R., Hajdas, I., Bonani, G., 2001. Persistent solar influence on North Atlantic climate during the Holocene. Science 294, 2130–2136.

Bond, G.C., Lotti, R., 1995. Iceberg discharges into the north Atlantic on millennial time scales during the last glaciation. Science 267, 1005–1010.

Born, A., Kageyama, M., Nisancioglu, K.H., 2010a. Warm nordic seas delayed glacial inception in scandinavia. Clim. Past. 6, 817–826.

Born, A., Nisancioglu, K.H., Braconnot, P., 2010b. Sea ice induced changes in ocean circulation during the Eemian. Clim. Dyn. 35, 1361–1371.

Born, A., Nisancioglu, K.H., Risebrobakken, B., 2011. Late Eemian warming in the Nordic Seas as seen in proxy data and climate models. Paleoceanography 26.

Capron, E., Govin, A., Stone, E.J., Masson-Delmotte, V., Mulitza, S., Otto-Bliesner, B., Rasmussen, T.L., Sime, L.C., Waelbroeck, C., Wolff, E.W., 2014. Temporal and spatial structure of multi-millennial temperature changes at high latitudes during the Last Interglacial. Quat. Sci. Rev. 103, 116–133.

Carlson, A.E., Stoner, J.S., Donnelly, J.P., Hillaire-Marcel, C., 2008. Response of the southern Greenland Ice Sheet during the last two deglaciations. Geology 36, 359–362.

Chapman, M.R., Shackleton, N.J., 1999. Global ice-volume fluctuations, North Atlantic ice-rafting events, and deep-ocean circulation changes between 130 and 70 ka. Geology 27, 795–798.

Cheng, H., Edwards, R.L., Broecker, W.S., Denton, G.H., Kong, X., Wang, Y., Zhang, R., Wang, X., 2009. Ice age terminations. Science 326, 248–252.

Clark, P.U., Alley, R.B., Pollard, D., 1999. Northern hemisphere ice-sheet influences on global climate change. Science 286, 1104–1111.

Colville, E.J., Carlson, A.E., Beard, B.L., Hatfield, R.G., Stoner, J.S., Reyes, A.V., Ullman, D.J., 2011. Sr-Nd-Pb isotope evidence for ice-sheet presence on southern Greenland during the last interglacial. Science 333, 620–623.

Crucifix, M.C., Loutre, F., 2002. Transient simulations over the last interglacial period (126-115 kyr BP): feedback and forcing analysis. Clim. Dyn. 19, 417–433.

Cuny, J., Rhines, P.B., Niiler, P.P., Bacon, S., 2002. Labrador sea boundary currents and

the fate of the irminger sea water. J. Phys. Oceanogr. 32, 627–647.
Darling, K.F., Kucera, M., Kroon, D., Wade, C.M., 2006. A resolution for the coiling direction paradox in *Neogloboquadrina pachyderma*. Paleoceanography 21, PA2011.
de Vernal, A., Hillaire-Marcel, C., 2008. Natural variability of Greenland climate, vegetation, and ice volume during the past Million Years. Science 320, 1622–1625.
Dokken, T.M., Jansen, E., 1999. Rapid changes in the mechanism of ocean convection during the last glacial period. Nature 401, 458–461.
Drysdale, R.N., Zanchetta, G., Hellstrom, J.C., Fallick, A.E., McDonald, J., Cartwright, I., 2007. Stalagmite evidence for the precise timing of North Atlantic cold events during the early last glacial. Geology 35, 77–80.
Elliot, M., Labeyrie, L., Bond, G., Cortijo, E., Turon, J.-L., Tisnerat, N., Duplessy, J.-C., 1998. Millennial-scale iceberg discharges in the irminger basin during the last glacial period: relationship with the Heinrich events and environmental settings. Paleoceanography 13, 433–446.
Fronval, T., Jansen, E., 1997. Eemian and early Weichselian (140-60 ka) paleoceanography and paleoclimate in the nordic seas with comparisons to Holocene conditions. Paleoceanography 12, 443–462.
Fronval, T., Jansen, E., Bloemendal, J., Johnsen, S., 1995. Oceanic evidence for coherent fluctuations in Fennoscandian and Laurentide ice sheets on millennium timescales. Nature 374, 443.
Fronval, T., Jansen, E., Haflidason, H., Sejrup, J.P., 1998. Variability in surface and deep water conditions in the Nordic seas during the last interglacial period. Quat. Sci. Rev. 17, 963–985.
Funder, S., Kjeldsen, K.K., Kjær, K.H., Ó Cofaigh, C., 2011. Chapter 50-The Greenland ice sheet during the past 300,000 Years: a review. In: Jürgen Ehlers, P.L.G., Philip, D.H. (Eds.), Developments in Quaternary Sciences. Elsevier, pp. 699–713.
Galaasen, E.V., Ninnemann, U.S., Irvalı, N., Kleiven, H.F., Rosenthal, Y., Kissel, C., Hodell, D.A., 2014. Rapid reductions in North Atlantic deep water during the peak of the last interglacial period. Science 343, 1129–1132.
Govin, A., Braconnot, P., Capron, E., Cortijo, E., Duplessy, J.-C., Jansen, E., Labeyrie, L., Landais, A., Marti, O., Michel, E., Mosquet, E., Risebrobakken, B., Swingedouw, D., Waelbroeck, C., 2012. Persistent influence of ice sheet melting on high northern latitude climate during the early last interglacial. Clim. Past. 8, 483–507.
Hansen, J., Sato, M., Hearty, P., Ruedy, R., Kelley, M., Masson-Delmotte, V., Russell, G., Tselioudis, G., Cao, J., Rignot, E., Velicogna, I., Tormey, B., Donovan, B., Kandiano, E., von Schuckmann, K., Kharecha, P., Legrande, A.N., Bauer, M., Lo, K.W., 2016. Ice melt, sea level rise and superstorms: evidence from paleoclimate data, climate modeling, and modern observations that 2 °C global warming could be dangerous. Atmos. Chem. Phys. 16, 3761–3812.
Hátún, H., Sandø, A.B., Drange, H., Hansen, B., Valdimarsson, H., 2005. Influence of the Atlantic subpolar Gyre on the thermohaline circulation. Science 309, 1841–1844.
Hibbert, F.D., Austin, W.E.N., Leng, M.J., Gatliff, R.W., 2010. British Ice Sheet dynamics inferred from North Atlantic ice-rafted debris records spanning the last 175 000 years. J. Quat. Sci. 25, 461–482.
Hillaire-Marcel, C., de Vernal, A., Bilodeau, G., Wu, G., 1994. Isotope stratigraphy, sedimentation rates, deep circulation, and carbonate events in the Labrador Sea during the last ~ 200 ka. Can. J. Earth Sci. 31, 63–89.
Hodell, D.A., Minth, E.K., Curtis, J.H., McCave, I.N., Hall, I.R., Channell, J.E.T., Xuan, C., 2009. Surface and deep-water hydrography on Gardar Drift (Iceland Basin) during the last interglacial period. Earth Planet. Sci. Lett. 288, 10–19.
Houghton, R.W., Visbeck, M.H., 2002. Quasi-decadal salinity fluctuations in the Labrador sea. J. Phys. Oceanogr. 32, 687–701.
Hutson, W.H., 1980. The Agulhas current during the late pleistocene: analysis of modern faunal analogs. Science 207, 64–66.
Irvalı, N., Ninnemann, U.S., Galaasen, E.V., Rosenthal, Y., Kroon, D., Oppo, D.W., Kleiven, H.F., Darling, K.F., Kissel, C., 2012. Rapid switches in subpolar North Atlantic hydrography and climate during the Last Interglacial (MIS 5e). Paleoceanography 27, PA2207.
Jansen, E., Fronval, T., Rack, F., Channell, J.E.T., 2000. Pliocene-pleistocene ice rafting history and cyclicity in the nordic seas during the last 3.5 Myr. Paleoceanography 15, 709–721.
Jennings, A.E., Hald, M., Smith, M., Andrews, J.T., 2006. Freshwater forcing from the Greenland Ice Sheet during the Younger Dryas: evidence from southeastern Greenland shelf cores. Quat. Sci. Rev. 25, 282–298.
Johannessen, T., Jansen, E., Flatøy, A., Ravelo, A.C., 1994. The relationship between surface water masses, oceanographic fronts and paleoclimatic proxies in surface sediments of the Greenland, Iceland Norwegian Seas. In: Zahn, R., Pedersen, T.F., Kaminski, M.A., Labeyrie, L.D. (Eds.), Carbon Cycling in the Glacial Ocean: Constraints on the Ocean's Role in Global Change, pp. 61–86.
Jonkers, L., Brummer, G.-J.A., Peeters, F.J.C., van Aken, H.M., De Jong, M.F., 2010. Seasonal stratification, shell flux, and oxygen isotope dynamics of left-coiling *N. pachyderma* and *T. quinqueloba* in the western subpolar North Atlantic. Paleoceanography 25, PA2204.
Khodri, M., Leclainche, Y., Ramstein, G., Braconnot, P., et al., 2001. Simulating the amplification of orbital forcing by ocean feedbacks in the last glaciation. Nature 410, 570.
King, E.L., Sejrup, H.P., Haflidason, H., Elverhøi, A., Aarseth, I., 1996. Quaternary seismic stratigraphy of the North Sea Fan: glacially-fed gravity flow aprons, hemipelagic sediments, and large submarine slides. Mar. Geol. 130, 293–315.
Kohfeld, K.E., Fairbanks, R.G., Smith, S.L., Walsh, I.D., 1996. *Neogloboquadrina pachyderma* (sinistral coiling) as paleoceanographic tracers in polar oceans: evidence from Northeast Water Polynya plankton tows, sediment traps, and surface sediments. Paleoceanography 11, 679–699.
Kozdon, R., Eisenhauer, A., Weinelt, M., Meland, M.Y., Nürnberg, D., 2009. Reassessing Mg/Ca temperature calibrations of Neogloboquadrina pachyderma (sinistral) using paired delta(44/40)Ca and Mg/Ca measurements. Geochem. Geophys. Geosyst 10, 1–14.
Kucera, M., Weinelt, M., Kiefer, T., Pflaumann, U., Hayes, A., Weinelt, M., Chen, M.-T., Mix, A.C., Barrows, T.T., Cortijo, E., Duprat, J., Juggins, S., Waelbroeck, C., 2005. Reconstruction of sea-surface temperatures from assemblages of planktonic foraminifera: multi-technique approach based on geographically constrained calibration data sets and its application to glacial Atlantic and Pacific Oceans. Quat. Sci. Rev. 24, 951–998.
Landais, A., Masson-Delmotte, V., Jouzel, J., Raynaud, D., Johnsen, S., Huber, C., Leuenberger, M., Schwander, J., Minster, B., 2006. The glacial inception as recorded in the NorthGRIP Greenland ice core: timing, structure and associated abrupt temperature changes. Clim. Dyn. 26, 273–284.
Laskar, J., Robutel, P., Joutel, F., Gastineau, M., Correia, A.C.M., Levrard, B., 2004. A long-term numerical solution for the insolation quantities of the Earth. Astron. Astrophys. 428, 261–285.
Lehman, S.J., Sachs, J.P., Crotwell, A.M., Keigwin, L.D., Boyle, E.A., 2002. Relation of subtropical Atlantic temperature, high-latitude ice rafting, deep water formation, and European climate 130,000-60,000 years ago. Quat. Sci. Rev. 21, 1917–1924.
Lisiecki, L.E., Raymo, M.E., 2005. A Pliocene-Pleistocene stack of 57 globally distributed benthic δ18O records. Paleoceanography 20. PA1003.
Mackensen, A., Hubberten, H.W., Bickert, T., Fischer, G., Fütterer, D.K., 1993. The δ13C in benthic foraminiferal tests of Fontbotia wuellerstorfi (schwager) relative to the δ13C of dissolved inorganic carbon in southern ocean deep water: implications for glacial ocean circulation models. Paleoceanography 8, 587–610.
Mangerud, J., Jansen, E., Landvik, J.Y., 1996. Late cenozoic history of the scandinavian and barents sea ice sheets. Glob. Planet. Change 12, 11–26.
Masson-Delmotte, V., Braconnot, P., Hoffmann, G., Jouzel, J., Kageyama, M., Landais, A., Lejeune, Q., Risi, C., Sime, L., Sjolte, J., Swingedouw, D., Vinther, B., 2011. Sensitivity of interglacial Greenland temperature and d18O: ice core data, orbital and increased CO2 climate simulations. Clim. Past. 7, 1041–1059.
McCartney, M.S., 1992. Recirculating components to the deep boundary current of the northern North Atlantic. Prog. Oceanogr. 29, 283–383.
McManus, J.F., Bond, G.C., Broecker, W.S., Johnsen, S., Labeyrie, L., Higgins, S., 1994. High-resolution climate records from the North Atlantic during the last interglacial. Nature 371, 326.
McManus, J.F., Oppo, D.W., Keigwin, L.D., Cullen, J.L., Bond, G.C., 2002. Thermohaline circulation and prolonged interglacial warmth in the North Atlantic. Quat. Res. 58, 17–21.
Meland, M.Y., Jansen, E., Elderfield, H., Dokken, T.M., Olsen, A., Bellerby, R.G.J., 2006. Mg/Ca ratios in the planktonic foraminifer *Neogloboquadrina pachyderma* (sinistral) in the northern North Atlantic/Nordic Seas. Geochem. Geophys. Geosyst. 7, Q06P14.
Mokeddem, Z., McManus, J.F., Oppo, D.W., 2014. Oceanographic dynamics and the end of the last interglacial in the subpolar North Atlantic. Proc. Natl. Acad. Sci. 111, 11263–11268.
NEEM community members, 2013. Eemian interglacial reconstructed from a Greenland folded ice core. Nature 493, 489–494.
Oppo, D.W., Keigwin, L.D., McManus, J.F., Cullen, J.L., 2001. Persistent suborbital climate variability in marine isotope stage 5 and Termination II. Paleoceanography 16, 280–292.
Oppo, D.W., McManus, J.F., Cullen, J.L., 2006. Evolution and demise of the last interglacial warmth in the subpolar North Atlantic. Quat. Sci. Rev. 25, 3268–3277.
Otto-Bliesner, B.L., Marshall, S.J., Overpeck, J.T., Miller, G.H., Hu, A.X., CAPE Last Interglacial Project members, 2006. Simulating arctic climate warmth and icefield retreat in the last interglaciation. Science 311, 1751–1753.
Parrenin, F., Barnola, J.M., Beer, J., Blunier, T., Castellano, E., Chappellaz, J., Dreyfus, G., Fischer, H., Fujita, S., Jouzel, J., Kawamura, K., Lemieux-Dudon, B., Loulergue, L., Masson-Delmotte, V., Narcisi, B., Petit, J.R., Raisbeck, G., Raynaud, D., Ruth, U., Schwander, J., Severi, M., Spahni, R., Steffensen, J.P., Svensson, A., Udisti, R., Waelbroeck, C., Wolff, E., 2007. The EDC3 chronology for the EPICA Dome C ice core. Clim. Past. 3, 485–497.
Prell, W.L., 1985. The Stability of Low-Latitude Sea Surface Temperatures: an Evaluation of the CLIMAP Reconstruction with Emphasis on the Positive SST Anomalies. U. S. Dep. of Energy, Washington, D.C, p. 60.
Prell, W.L., Martin, A., Cullen, J., Trend, M., 1999. The Brown University Foraminiferal Data Base, IGBP PAGES/World Data Center-A for Paleoclimatology Data Contribution Series # 1999-027. NOAA/NGDC Paleoclimatology Program, Boulder CO, USA.
Rasmussen, T.L., Thomsen, E., Kuijpers, A., Wastegård, S., 2003. Late warming and early cooling of the sea surface in the Nordic seas during MIS 5e (Eemian Interglacial). Quat. Sci. Rev. 22, 809–821.
Rosenthal, Y., Field, M.P., Sherrell, R.M., 1999. Precise determination of element/calcium ratios in calcareous samples using sector field inductively coupled plasma mass spectrometry. Anal. Chem. 71, 3248–3253.
Rosenthal, Y., Perron-Cashman, S., Lear, C.H., Bard, E., Barker, S., Billups, K., Bryan, M., Delaney, M.L., deMenocal, P.B., Dwyer, G.S., Elderfield, H., German, C.R., Greaves, M., Lea, D.W., Marchitto Jr., T.M., Pak, D.K., Paradis, G.L., Russell, A.D., Schneider, R.R., Scheiderich, K., Stott, L., Tachikawa, K., Tappa, E., Thunell, R., Wara, M., Weldeab, S., Wilson, P.A., 2004. Interlaboratory comparison study of

Mg/Ca and Sr/Ca measurements in planktonic foraminifera for paleoceanographic research. Geochem. Geophys. Geosyst. 5, Q04D09.
Rousseau, D.D., Kukla, G., McManus, J., 2006. What is what in the ice and the ocean? Quat. Sci. Rev. 25, 2025–2030.
Ruddiman, W.F., 1977. Late Quaternary deposition of ice-rafted sand in the subpolar North Atlantic (lat 40{degrees} to 65{degrees}N). Geol. Soc. Am. Bull. 88, 1813–1827.
Sánchez Goñi, M.F., Loutre, M.F., Crucifix, M., Peyron, O., Santos, L., Duprat, J., Malaizé, B., Turon, J.L., Peypouquet, J.P., 2005. Increasing vegetation and climate gradient in Western Europe over the Last Glacial Inception (122-110 ka): data-model comparison. Earth Planet. Sci. Lett. 231, 111–130.
Sejrup, H.P., Larsen, E., Landvik, J., King, E.L., Haflidason, H., Nesje, A., 2000. Quaternary glaciations in southern Fennoscandia: evidence from southwestern Norway and the northern North Sea region. Quat. Sci. Rev. 19, 667–685.
Shackleton, N.J., Chapman, M., Sánchez Goñi, M.F., Pailler, D., Lancelot, Y., 2002. The classic Marine Isotope Substage 5e. Quat. Res. 58, 14–16.
Shackleton, N.J., Hall, M.A., Vincent, E., 2000. Phase relationships between millennial-scale events 64,000-24,000 years ago. Paleoceanography 15, 565–569.
Shackleton, N.J., Sánchez Goñi, M.F., Pailler, D., Lancelot, Y., 2003. Marine Isotope Substage 5e and the Eemian Interglacial. Global Planet. Change 36, 151–155.
Simstich, J., Sarnthein, M., Erlenkeuser, H., 2003. Paired δ18O signals of Neogloboquadrina pachyderma (s) and Turborotalita quinqueloba show thermal stratification structure in Nordic Seas. Mar. Micropaleontol. 48, 107–125.
Sirocko, F., Seelos, K., Schaber, K., Rein, B., Dreher, F., Diehl, M., Lehne, R., Jager, K., Krbetschek, M., Degering, D., 2005. A late Eemian aridity pulse in central Europe during the last glacial inception. Nature 436, 833–836.
Skinner, L.C., Shackleton, N.J., 2005. An Atlantic lead over Pacific deep-water change across Termination I: implications for the application of the marine isotope stage stratigraphy. Quat. Sci. Rev. 24, 571–580.
Stirling, C.H., Esat, T.M., Lambeck, K., McCulloch, M.T., 1998. Timing and duration of the Last Interglacial: evidence for a restricted interval of widespread coral reef growth. Earth Planet. Sci. Lett. 160, 745–762.
Swift, J.H., Aagaard, K., 1981. Seasonal transitions and water mass formation in the Iceland and Greenland seas. Deep Sea Research Part A. Oceanogr. Res. Pap. 28, 1107–1129.
Thompson, W.G., Allen Curran, H., Wilson, M.A., White, B., 2011. Sea-level oscillations during the last interglacial highstand recorded by Bahamas corals. Nat. Geosci. 4, 684–687.
Thompson, W.G., Goldstein, S.L., 2006. A radiometric calibration of the SPECMAP timescale. Quat. Sci. Rev. 25, 3207–3215.
Tolderlund, D.S., Bé, A.W.H., 1971. Seasonal distribution of planktonic foraminifera in the western North Atlantic. Micropaleontology 17, 297–329.
Tzedakis, P.C., Wolff, E.W., Skinner, L.C., Brovkin, V., Hodell, D.A., McManus, J.F., Raynaud, D., 2012. Can we predict the duration of an interglacial? Clim. Past. 8, 1473–1485.
Van Nieuwenhove, N., Bauch, H.A., Andruleit, H., 2013. Multiproxy fossil comparison reveals contrasting surface ocean conditions in the western Iceland Sea for the last two interglacials. Palaeogeogr. Palaeoclimatol. Palaeoecol. 370, 247–259.
Van Nieuwenhove, N., Bauch, H.A., Eynaud, F., Kandiano, E., Cortijo, E., Turon, J.-L., 2011. Evidence for delayed poleward expansion of North Atlantic surface waters during the last interglacial (MIS 5e). Quat. Sci. Rev. 30, 934–946.
Wold, C.N., 1994. Cenozoic sediment accumulation on drifts in the northern North-Atlantic. Paleoceanography 9, 917–941.
Wright, A.K., Flower, B.P., 2002. Surface and deep ocean circulation in the subpolar North Atlantic during the mid-Pleistocene revolution. Paleoceanography 17, 1068.